18/04/2013

Luminescence dating of sediments from a Palaeolithic site associated with a solution feature on the North Downs of Kent, UK

I. K. Bailiff[1]*, S. G. Lewis[2], H. C. Drinkall[1] and M. J. White[1]

[1]Department of Archaeology, Durham University, South Road, Durham DH1 3LE, UK

[2]School of Geography, Queen Mary, University of London, Mile End Road, London E1 4NS, UK

Keywords: luminescence dating, single grain, sediment, solution hollow, palaeolithic, upland

*Corresponding author

Abstract

Optically stimulated luminescence (OSL) dating has been applied to determine the burial age of sediment horizons within a sequence containing Lower Palaeolithic artefacts on an upland site associated with a solution feature (doline) at West Cliffe, located on the North Downs in Kent, UK. The study makes use of a novel extension of the single aliquot OSL measurement procedure to investigate the nature of significant overdispersion in equivalent dose values with very small aliquots of quartz inclusions, enabling single grain resolution to be approached with ~90 μm diameter quartz extracted from the relatively fine-grained brickearth. A detailed examination of the uniformity of the distribution of radionuclide sources in the sampled volumes was also performed and this included the application of a spatially-resolved technique for beta dose rate measurement. The OSL ages, obtained for the burial of brickearth positioned stratigraphically below and above a clay and flint clast layer containing the artefacts and debitage, place the deposition of the artefacts to between ca 140 and 80 ka ago. This is significantly later than indicated by the artefact typology (>300 ka) and contrary to the expectation of *in situ* burial indicated by earlier research in this region. If displacement occurred on other upland sites this finding has important implications for establishing the timing of hominin use of the upland areas which, beyond broad attribution to Lower or Middle Palaeolithic origin, is uncertain and similar doubts apply to the interpretation of the environments that prevailed.

1. Introduction

Palaeolithic sites formed in association with a solution feature, such as a doline or a sinkhole, provide a potentially rich source of preserved archaeological remains. Sites of this type have been investigated, for example, in the Chalk uplands of southern Britain (Wood Hill, Scott-Jackson 2000; Caddington, Sampson 1978), in limestone karsts of the Duero River Basin and adjacent plateaus in north-central Spain (Valdecampaňa 4; Diez-Martín et al., 2008), in northern France on interfluvial plateaux in the Somme basin (Gentilles, Tuffreau et al., 2008) and in south-west France (Creysse; Bourguignon et al., 2008; Guibert et al., 2008). Hominins were probably attracted to these sites by the availability of raw material, water supply from ponds formed in the solution hollows and the associated resources that could be utilised from upland locations. The importance of these upland sites lies in providing insights into hominin activities away from the river valleys (Ashton et al., 2006), though their geographical and stratigraphical isolation can present significant challenges for correlation and dating in the absence of suitable materials. Where burnt lithic materials associated with tool manufacture are recovered from either the solution features or near-surface deposits, thermoluminescence (TL) dates have provided a means of assigning production to a particular period. At the site of Wood Hill, located on a solution feature, TL dates of 350±26 ka and 200±33 ka were obtained for burnt flint recovered from two separate trenches, the earlier of which supports Lower Palaeolithic occupation (Scott-Jackson, 2000). Similarly, a TL date of 140±11 ka for burnt quartzite recovered from the sinkhole at Valdecampaňa 4, and also three more cautiously presented TL dates for surface survey material ranging from 130 - 260 ka, confirmed prolonged use of the landscape during the Later Middle Pleistocene (Diez-Martin et al., 2008).

In the absence of burnt lithics, optically stimulated luminescence (OSL) techniques applied to the sedimentary horizons in which the lithics occur offer one of the few means of potentially dating these sites, providing the luminescence characteristics of the minerals and the process of deposition are suitable. At Gentilles, an infrared stimulated luminescence (IRSL) burial age

of 194±21 ka was obtained with the fine grain fraction of reworked calcareous loess that formed the horizon from which horse bone was recovered (Tuffreau et al., 2008). However, in the case of solution hollows the processes that lead to their filling, involving episodic input and reworking of sediment during periods of active solution formation and including subsequent erosional processes, are likely to produce potentially complex sedimentary sequences, and this may account for the generally limited application of luminescence to the dating of the sedimentary fill of such features. In this study we examined an upland Lower Palaeolithic site at West Cliffe that is 4 km SW of Wood Hill and similarly located on a solution feature. However, unlike Wood Hill, no burnt flint was recovered during the excavation and consequently OSL dating was applied to obtain burial ages for horizons within the solution feature containing the cultural deposits. A detailed micromorphological investigation performed at Wood Hill indicated that the solution process had caused the sediment horizons within the upper part of the hollow feature to be slowly lowered without significant lateral transport. It was concluded that the Palaeolithic artefacts, manufactured or discarded within the solution hollow, were eventually buried *in situ* (Scott-Jackson, 2000; Scott-Jackson and Walkington, 2005). This finding has led to the general assumption that similar processes occurred on sites of this type in SE England. By sampling the sediment horizons in the solution feature at West Cliffe we aimed to investigate whether the artefacts had remained in a primary context of Lower Palaeolithic age. If significant post-depositional disturbance had occurred it would have important implications for the interpretation of lithic scatters at West Cliffe and also those found in comparable situations in other upland locations.

An initial evaluation of the potential of applying OSL (Drinkall, 2005) to sediments collected from three key sedimentary units produced burial ages of less than 100 ka using the polymineral fine-grain technique (Aitken, 1998). Although these tests detected a degree of anomalous fading associated with the feldspar fraction, the OSL ages were significantly younger than the Lower Palaeolithic artefact typology (> ca 300 ka), raising doubts that they were *in situ* deposits as had been concluded in the Wood Hill study. The investigation was

continued by performing measurements with single aliquots of coarse quartz grains to avoid the problems of anomalous fading (Wintle, 1973) and, to examine for the possibility of redeposition of the lithics, by investigating the potential for single grain measurements (Duller, 2008). Recent developments in single grain OSL techniques, which are normally applied using coarse grains (>200 μm dia.), provide a means of examining these issues by assessing the extent to which temporal heterogeneity exists in sediment sequences with complex depositional histories. This is achieved by an analysis of the distribution of values of the equivalent dose, D_e, determined for individual grains, where D_e is the numerator in the luminescence age equation (Age= $D_e/\dot{D}_{tot}$; $\dot{D}_{tot}$ is the dose rate). The approach has been applied in various studies (e.g., Jacobs et al, 2012; Arnold et al., 2009; Bateman, 2007) to resolve components in the single grain D_e distribution, where each component is associated with a depositional phase within a site formation model, and to calculate the burial age for those components. Although the use of quartz has been favoured for application to Palaeolithic sites to avoid the effects of anomalous fading, its range had been considered to be generally insufficient for dating Lower Palaeolithic horizons. Nonetheless, recent comparisons of OSL ages for coarse grain quartz from fluvial deposits with independent dating evidence have produced good agreement (Murray et al., 2008), extending to ca 450 ka providing the fast decay component of the OSL signal is measured (Pawley et al., 2010). The sites in the latter study were in the Thames Valley, UK, and while the upper limit of the dating range is governed by the characteristics of the quartz and the level of the dose rate, these comparisons indicate the potential viability of using quartz OSL techniques for investigating solution features with evidence of Lower Palaeolithic occupation and provided encouragement to proceed with the use of quartz. However the upper grain size of the sediments within the sampled contexts at West Cliffe was limited to ca.120 μm diameter, significantly smaller than the minimum size for HF etched grains measured in a single grain reader (>180 μm dia.). The development of an alternative procedure for measuring the OSL from individual quartz grains within the size range available formed the part of the continued investigation. Also the

uniformity of the distribution of radionuclides contributing to the beta dose was examined as a potential source of dispersion when examining the D_e distributions. We first summarise the nature of the archaeological evidence within its sedimentary contexts and the interpretation of the site formation processes.

2. The site and geoarchaeological context of the OSL samples

The site of West Cliffe, St. Margaret's (National Grid Reference TR 3745 4905), is located at an elevation of +95 m OD on a ridge of the North Downs between Dover and Deal (Supplementary Material Fig. SM1). It is one of a group of Palaeolithic sites, discovered by the Dover Archaeological Group (Halliwell and Parfitt, 1995; Parfitt and Halliwell, 1996; Scott-Jackson, 2000). These sites are situated in upland locations in S. Britain which are (with the exception of Wood Hill) difficult to tie to any accepted relative chronology (e.g., Bridgland, 1994; Schreve, 2001) owing to their geographical location outside of fluvial basins, and are mostly assigned typologically to a generic Lower Palaeolithic date. At West Cliffe over 700 heavily patinated and stained flint artefacts, including Acheulean handaxes, cores and flakes, were recovered during fieldwalking. The artefacts at first appeared to be clustered around a depression in the land surface, indicative of an active solution feature (doline). West Cliffe ultimately yielded over a thousand artefacts, of which over 650 were from excavated contexts. Typologically the assemblage is Lower Palaeolithic (>300ka) in character, and includes handaxes, roughouts, flakes, cores, core tools, and flake tools including scrapers, retouched flakes and notches, but mainly comprising debitage.

Three conjoining solution hollows are identifiable in the area (A, B and C in Fig. 1) and the Chalk surface elevation and thickness of the overlying sediments are locally very variable. This indicates that karst processes are forming localised solution features. The depression visible in the land surface today (A, in Fig. 1) corresponds to a sub-surface depression in the Chalk and a thick sedimentary fill (solution doline). This feature is potentially still forming today. Despite the surface distribution of artefacts at the margin of this feature, further investigation revealed

that the artefact concentration is associated with the margins of one (B) of two older hollows (B and C, Fig. 1). These features have no visible surface depression and are interpreted as inactive dolines.

The sediments overlying the Chalk comprise two units; Clay-with-flints and a series of predominantly silty sediments referred to here as ‘brickearth’. The Clay-with-flints (sensu stricto, c.f. Loveday, 1962) is the thin clay at the interface of the Chalk with the overlying sediments, and ranges in thickness from 5 cm to over 50 cm; it is typically dark brown in colour and contains some large flint clasts including Bullhead flint pebbles. The brickearth, which infills the solution features, is a massive, structureless and stoneless, brown coloured, silt-dominated unit of variable thickness. The silty texture of the brickearth suggests that it is partly of wind-blown origin, though reworking and mixing with other fine-grained materials by alluvial and/or colluvial processes has probably occurred.

Field excavations identified a sub-aerially weathered flint pavement at a shallow depth beneath the ground surface as the source of the Lower Palaeolithic artefacts collected in the original fieldwalking. This pavement dipped towards hollow B where a layer of flint cobbles in a brown matrix, dipping at an angle of ca 45° and representing the continuation of the pavement, contains the main artefact concentration (Fig. 2a,b). Brickearth occurs above and below this cobble layer. The excavations also showed evidence of rill and pipe formation, slumping and sediment displacement (Supplementary Material, Fig. SM2a,b).

The field evidence suggests that site formation can be attributed to Chalk solution and infilling of the resulting depressions with predominantly fine-grained sediments, but also comprising flint cobbles, including Palaeolithic artefacts. Localised Chalk solution resulted in the formation of a depression in the landscape, which may have retained water at least seasonally, and around the margins of which the discard of lithic artefacts by hominin activity occurred. During phases of cold climate conditions Chalk solution processes ceased and periglacial conditions

dominated, with the development of permafrost during periods of most severe conditions and a seasonally thawed active layer which caused associated disturbance of the surface layers, including any artefacts present. The rill features provide a conduit for surface water and sediment movement (Torri et al., 1987; Waltham et al., 2005: 66) and transport of larger stones, including artefacts, into the solution feature during periods of higher velocity flow. Loess accumulation and reworking into the hollow resulted in infilling of the basin. Renewed Chalk solution under warm climate conditions resulted in further development of the depression and sediments already in the doline were more deeply buried in the feature, with new material also contributing to the infill. The pipes and rills leading into a solution feature periodically can become blocked by sediment and stones (Jennings, 1985; Ford and Williams, 1989), allowing water to accumulate in the depression forming a pond, and it is likely that this would have been the prevailing condition at the time of hominin occupation. A situation was eventually reached when the doline ceased to be active, possibly resulting from a reduction in solution as the depth of the feature increased and groundwater flow to the solution front was impeded by the greater thickness of the infilling sediments. A new feature formed adjacent to it and remains visible as a depression in the landscape today.

Samples for OSL were taken from a section (04/04) cut south-west to north-east through the cobble layer (Fig. 2b). This section revealed the layer of flint cobbles encapsulated within a brown clay matrix (10YR 4/4) dipping to the south-east, above a brown silt/clay with greenish mottling (10YR 5/6), and overlain by a massive structureless deposit of yellowish brown silt-clay (10YR 6/6) containing two surfaces of black (manganese) staining. Three OSL samples were obtained by driving lengths of 50 mm dia. thin-walled metal coring tube into the cleaned face of the section (Fig. 2b). One sample was from the sediment below the cobble layer (316-1) at a depth of 1.25 m below the surface, the second from above the artefact horizon (316-2), in the main body of the yellowish brown silt-clay (depth, 1.20 m) and the final sample (316-3) was taken from just above an upper black manganese stain (depth, 1.15 m).

3. OSL investigation

3.1 Methodology

The experimental procedures applied to determine the equivalent dose D_e, discussed in further detail below, were based on a single aliquot regeneration (SAR) measurement sequence, initially with small aliquots (SA) and subsequently with very small aliquots (VSA) that typically contained less than 100 grains. For the latter, an additional experimental stage was introduced following the completion of the SAR sequence, where the distribution of OSL within each aliquot of etched quartz grains deposited on the stainless steel measurement disc, was recorded using an OSL scanner (Bailiff and Mikhailik, 2003). This enabled the number of brightly emitting grains to be identified and, by adjustment of the aliquot size, the production of discs containing a dominant individual bright grain.

3.2 Sample preparation

Coarse quartz grains were extracted following the procedures developed for the quartz inclusion technique (Aitken, 1998) and all sample preparation was performed under subdued red lighting conditions. Following the removal of carbonates (using 15% HCl), the sieved fraction was etched in HF (40%, 45 mins), immersed in HCl (40%) for 45 mins to remove fluoride precipitates, and finally re-sieved, with appropriate washing procedures being applied at each stage. For all three samples, the largest crystalline grains available in sufficient quantity were contained in the 90-150 μm fraction, with diameters biased towards the lower end of this range. Following HF treatment a high proportion of the grains passed through a 90 μm sieve, but inspection of the grains indicated that they were greater than ca 75 μm in diameter. Aliquots of the etched grains were deposited onto stainless steel discs that had been lightly sprayed with silicone oil, taking care to disperse the grains to avoid clustering. Before use all discs had been checked for the absence of background signal interference by applying

a beta dose of ca 300 Gy, a preheat (260°C) and measuring the response to optical stimulation.

3.3 Luminescence instrumentation

A TL-DA-12 semi-automated reader (Risø National Laboratory, Denmark) with a blue diode array stimulation source (470 nm; ~35 mW cm^{-2}) was used to measure the OSL, detected after passing through a Hoya U340 filter (7.5 mm thickness). The OSL decay curve was recorded for typically 20 s while maintaining a sample temperature of 125 ºC during stimulation to prevent retrapping of charge by traps associated with the 110 °C TL peak. The photon counter interval was set to 200 ms for SAR measurements, although for some of the initial tests it was 1s; to generate data suitable for conversion to pseudo linear modulation (LM) OSL curves, the decay curves were measured with a counter interval of 10 ms. TL signals were measured (heating rate, 5 ºC s^{-1}) with the detector configuration for OSL measurements. Laboratory β doses were administered to aliquots using a $^{90}Sr/^{90}Y$ β source mounted on the reader that had been calibrated against a secondary standard ^{60}Co source (Göksu et al., 1995; periodically checked with gamma photon irradiated granular quartz; the dose rate in Jan. 2012 was 3.06 Gy min^{-1}).

The distribution of OSL from grains within very small aliquots (~0.1 mg) was measured using an OSL scanner, the design of which has been described previously (Bailiff and Mikhailik, 2003). Within the scanner a laser beam (all lines, Argon-ion) is focused onto the sample disc located on the horizontal surface of an X-Y stage. A conventional PMT detection system is mounted directly above the disc. By programmed movement of the motor-controlled stage and shutter-controlled exposure to the laser beam, the OSL is measured at 1600 points within a scanned area of 10 x 10 mm; four discs are normally measured in one scan (20 x 20 mm).

3.4 Measurement and analysis procedures

The cumulative absorbed dose, D_e, was determined using a single aliquot regeneration (SAR) OSL procedure, similar to that described by Murray and Wintle (2000; 2003), but where the corrections for sensitivity change and thermal transfer are handled differently (Table 1). The test dose in the SAR protocol was replaced by a monitor dose of ca 200 Gy and five levels of regenerative dose were applied within the range ca 100-650 Gy. A second preheat and OSL decay curve measurement (referred to as a pre-heat monitor, PHM) was included in the sequence to examine the OSL signal arising from recuperation, and to define the background signal. During the first preheat before this pair of OSL measurements the TL was also recorded to monitor changes in TL sensitivity. Aliquots with recycling and IR depletion ratios (Wintle and Murray, 2006) greater than 15% were excluded from further analysis.

The OSL signal, shown in the dose response plots discussed below, corresponds to the counts recorded during the initial 800 ms of the OSL decay curve, and the same interval was used for the background, PHM, signal (referred to as PBG, preheat background). In view of the observations that have been made regarding the potential contribution to the initial part of the OSL decay curve from a medium decay component with a relatively short half life (Li and Li, 2006; Steffen et al., 2009), the early background (EBG) subtraction procedure (Ballarini et al., 2007; Cunningham and Wallinga, 2010) was also applied, using signal integration intervals of 0-800 ms and 800-1600 ms for signal and background respectively. The ratio of the D_e values calculated using EBG and PBG subtraction was employed to screen aliquots for the presence of the medium decay component. Where the central value of the mean ratio exceeded its 2σ range, the aliquot was considered to have a potentially intrusive medium decay component and not included in the calculation of the weighted mean value of D_e. The calculation of the FAST Ratio (Durcan and Duller, 2010) was also included in the OSL signal analysis to detect the influence of the medium decay component in the OSL signal, but for most of the very small aliquots tested the uncertainty in the ratio was significant due to statistical fluctuation associated with the OSL signal recorded within the time range selected for the medium component.

The dose recovery experiment (Wintle and Murray, 2006) was applied to test the evaluation of a known laboratory dose following laboratory replication of the optical resetting process. The trapped charge was depleted at room temperature (RT) using the blue LED source and, following storage for 10 ks to remove phototransferred charge in traps associated with the 110 °C TL peak, any residual charge in the traps used for dosimetry was removed by a further OSL measurement at RT. The experimentally determined value of the dose applied (~200-600 Gy) was then obtained using the SAR procedure.

Dose response curves (either a single saturating exponential, SSE, or a saturating exponential plus linear function, SEPL; Berger, 1990) were fitted to the sensitivity corrected OSL signals by applying a Monte Carlo (MC) simulation, combined with a least squares algorithm incorporated in a Microsoft Excel sheet employing Solver and MCSimSolver (Barreto and Howland, 2006) add-ins. For each step of the Monte Carlo simulation, the value of the OSL signal intensity was drawn from a normal distribution with a relative standard deviation derived from the (Poisson) uncertainty in the net integrated counts. The standard deviation of the distribution of D_e values calculated by the simulation (50 cycles) was used as the estimate of uncertainty in D_e. The analysis of D_e distributions included the use of the central dose (CDM; originally referred to as CAM, Central Age Model) and finite mixture statistical models (FMM) developed by Galbraith (2005).

The uncertainty in the age ($\pm 1\sigma$) was calculated by propagating the errors associated with the experimental measurements, including calibrations and conversion factors, following a procedure similar to that described by Aitken (1985).

3.4.1 Aliquot size

Measurements of the OSL characteristics were initially performed with single aliquots (ca 1 mg) to obtain strong signal intensities provided by multiple bright grains. Subsequently very small aliquots (containing ca 50 -100 grains) were used to investigate single grain OSL measurements; they were deposited onto discs using a dental point that had been dipped into

the etched sample. A count of the number of brightly emitting grains in each aliquot was obtained by administering a beta dose at the end of the SAR sequence and measuring the spatial distribution of the OSL using the scanner. The amount of quartz was progressively adjusted with the aim of obtaining one bright grain per disc. Aliquots were first screened for OSL signal strength by measuring the natural OSL and, if sufficient, completing the SAR measurement sequence. Of the aliquots that produced luminescence of sufficient intensity, the number of individual bright grains detected by scanning was typically between 0 and 3 and, where no bright grains were resolved, the aliquot was categorised as multiple grain. Fig. 3 shows an example of a bright grain detected within an aliquot falling in the weaker range of OSL intensities observed with the West Cliffe samples. While the relative brightness of the OSL from an individual bright grain over the combined contribution from 'dim' grains can be established by spatially resolved measurements using a focused laser beam, a sufficient number of dim grains (i.e., with intensities falling within the levels of statistical fluctuation in the background signal) could make a non-negligible contribution to the OSL signal when recorded as a single aliquot under uniform LED stimulation. However, the proportionality found when comparing the OSL signal recorded by the scanner for each detected bright grain and the OSL signal recorded by the Risø reader in response to the first monitor dose indicates that the emission detected under LED stimulation was dominated by bright grain(s). For the weakest of the OSL signals produced by very small aliquots the limits of resolution of this approach are probably being approached.

FIG. 3

3.5 Results and discussion

3.5.1 OSL characteristics – small aliquots

The initial characterisation measurements were performed with small aliquots, the majority of which were from sample 316-2. A typical OSL decay curve measured with a single aliquot of sample 316-2 is shown in Fig. 4. The analysis of the pseudo LM-OSL curves (Bulur, 2000) confirmed the presence of a dominant fast decay and a medium decay component in aliquots

of all three samples, comparable to those published previously for quartz (Durcan and Duller, 2011; Pawley et al., 2010; Singarayer et al., 2003; Jain et al., 2003). The proportion of the medium decay component varied and appeared to be relatively much weaker in aliquots of sample 316-3. However, since the measurements were performed with small aliquots containing multiple bright grains to obtain sufficient signal intensity, the decay components observed represent a weighted sum of the decay curves for individual grains and the proportion of fast to medium decay components is likely to differ between grains. As observed by Adamiec (2005) and Duller (2012), the value of the decay constant is also likely to differ between individual grains.

FIG. 4

3.5.2 Dose response

The dependence of D_e on preheat temperature, T_P, was examined using temperatures of 260, 270 and 280 ºC (10s hold at T_P). The relatively high level of dispersion in D_e observed at each preheat temperature precluded the use of a precise plateau test, and a preheat temperature of 260 °C was selected for D_e evaluations on the basis of the behaviour of sample 316-2 [260 °C, 305±30 Gy (s.e., n=4); 270 °C, 310±15 Gy (n=15); 280 °C, 240±75 Gy (n=3)] and this preheat treatment was also applied to very small aliquots. An example of a typical SAR dose response plot is included in the Supplementary Material (Fig. SM3) where a single saturating exponential curve is fitted to the data.

The values of the recycling ratios, evaluated with a subset of aliquots where a full SAR sequence was repeated, illustrate satisfactory correction for sensitivity changes: 316-1, 1.0±0.01 (σ, n=6); 316-2, 0.95±0.06 (σ, n=27); 316-3, 0.99±0.08 (σ, n=4). Changes in OSL signal related to the IR depletion test were typically within 10% of unity.

For all three samples the dose response characteristics of aliquots varied significantly, as reflected in the distribution of the values of the dose-response parameter D_0 (Bailey, 2001). This variation is shown for sample 316-2 in Fig. 5a, where the value of D_0 ranges from ~150 to ~300 Gy; the distribution of D_e values is also wide (~200 Gy - ~500 Gy), but the majority lie

below the broken line that corresponds to the suggested working limit for D_e of $2D_0$ (Wintle and Murray, 2006). The calculation of D_e was performed using the PBG subtraction and a comparison of D_e values obtained using the EBG (signal, 0-800 ms and background, 800-1600 ms) and PBG subtraction procedures is shown in Fig. 5b. The value of the mean ratio is 1.05±0.07 (s.d., n=25). The relatively bright OSL from the small aliquots enabled a shorter EBG interval (signal, 0-200 ms; background, 200-400 ms) to be applied and this yielded a mean ratio of 1.04±0.13 (s.d., n=22), the greater dispersion reflecting poorer signal statistics resulting from the shorter integration interval. These plots indicate that for a high proportion of the small aliquots of sample 316-2 the signal obtained using a PBG subtraction with an 800 ms signal integration interval avoided significant intrusion by the medium decay component. The use of the EBG D_e data as the basis of a screening procedure, rather than providing directly D_e values for age determination, was found necessary because generally high values of the relative standard error (RSE) in D_e were obtained using an early background subtraction with the weaker OSL signals from very small aliquots.

FIG. 5

The weighted average values of D_e (CDM) and the values of the overdispersion for samples 316-1 (13%), -2 (26%) and -3 (21%) are given in Table 2a (cols 2-3), where it should be noted that relatively fewer aliquots of samples 316-1 and 3 were tested. Since the overdispersion for well bleached quartz grains is expected to be up to ca 20% in single grain determinations (Olley et al., 2004), and for small aliquots the overdispersion is reduced by the effects of inter-grain averaging (e.g., Cunningham at al., 2011), the values observed with small aliquots of the West Cliffe samples suggest that the sediments may have been partially bleached and/or buried in more than one phase. To investigate further the overdispersion in D_e, measurements were continued using very small aliquots (VSA), with the aim of approaching single grain resolution, by identifying aliquots with a dominant individual bright grain.

3.5.3 Dose recovery - very small aliquots

A single value of applied dose (D_a selected in the range 200-215 Gy) was initially administered to aliquots from each sample and the values of D_e obtained were plotted against the values of D_e calculated using the early subtraction procedure, EBG D_e (data for sample 316-1 shown in Fig. 6; equivalent plots for samples 316 -2 and -3 are shown in Supplementary Material Fig. SM4). Although the potential long-term instability in the medium decay component is not expected to affect the short-term laboratory dose recovery test, the comparison provides a means of testing the EBG subtraction procedure where relatively weaker OSL signals are obtained with very small aliquots.

FIG. 6

For all three samples the overdispersion (316-1, 13%; 316-2, 17%; 316-3, 12%) is significantly greater than that expected (0%), although, as discussed by Galbraith and Roberts (2012), in general there appears to be considerable variation in the overdispersion estimates obtained from dose recovery experiments with quartz tested in various studies. However the weighted average value of D_e (Table 2a, col. 6) is in reasonable agreement with the applied dose (D_a, col. 5) for samples 316-2 and 316-3 and some 10% higher for sample 316-1. The range of applied dose was extended (D_a= 408 and 612 Gy) for sample 316-1 (Fig. 7a) and, while the number of results is limited at these higher levels of dose, they show good agreement in recovering D_a at ca 400 Gy and indicate the onset of sub-linear growth by 600 Gy (Fig. 7b; Table 2a, col. 6). Although one aliquot from each of the two groups used for these higher dose recovery measurements produced a D_e value close to the limit of the working range ($2D_0$), the others were below it (average D_e/D_o = ~1.4). Hence the progressively increasing underestimation of the absorbed dose obtained at the higher levels of dose investigated (e.g., above 500 Gy) does not appear to be attributable to saturation of the dose response recorded by the SAR procedure. In recent work by Duller (2012) with quartz from a Palaeolithic site in Zambia, it was possible to eliminate overdispersion for applied doses of up to ca 150 Gy in dose recovery experiments by selecting grains with high values (>20) of the Fast Ratio. For the highest dose applied (178 Gy) the overdispersion rose to 27% and also the value of D_e underestimated the applied dose by some 20%. Hence it would appear that the effects are

similar to those observed with the West Cliffe quartz and likely to be observed in quartz from other regions.

FIG.7

3.5.4 Sensitivity changes- very small aliquots

One effect that could account for both underestimation and overdispersion observed in the dose recovery experiment is a change in OSL response during the first OSL measurement of the SAR sequence that is not corrected in the SAR analysis and this has been recently addressed by Singhvi et al. (2011). Using single aliquots they examined the use of the 110°C TL peak as a proxy for OSL sensitivity, providing a means of detecting and correcting for such changes if occurring only during the first measurement in the SAR procedure with single aliquots. A comparable approach was investigated with the West Cliffe samples by recording the TL signal (monitor) during the preheat (PH1, Table 1, note 2) following the administration of the applied beta dose, D_a, and following the first monitor dose ($\beta 1$, where $\beta 1 = D_a$) in the dose recovery experiment. The values of integrated TL signal (110 °C peak) recorded during the first (M1) and second (M2) measurements were used to calculate the monitor ratio (M2/M1), and the latter applied to correct the value of the natural OSL signal, I_N, for change in sensitivity during step 1 (i.e., $I_N' = M2 \cdot I_N/M1$). In Fig. 8 the values of D_e obtained using the SAR procedure (Table 1) are plotted against the values of D_e obtained after applying the monitor correction to I_N. Where the TL monitors indicate no significant sensitivity change, all the data points are expected to fall on the broken line and cluster at the coordinates 205, 205, corresponding to the value of D_a in this case. For three aliquots where the uncorrected D_e values (open circles) were significant outliers, the discrepancy is reduced, but the values of D_e for three other aliquots (open triangles) become outliers indicating that, for the West Cliffe quartz, the TL monitors do not appear to be a reliable proxy for OSL sensitivity change in the dose recovery test. Excluding the three aliquots where application of the monitor correction produced outliers, the average TL monitor ratio (M2/M1) was 0.93±0.07 (s.d., n=18).

TL measurements with single grain resolution would be required to establish whether any changes observed in OSL and TL response occur in the same individual grain(s).

3.5.5 Evaluation of burial dose - very small aliquots

Wide ranges of values of D_0 and D_e were obtained with aliquots, each containing an individual bright grain, from all three samples (shown in Fig. 9 for sample 316-1, and in Supplementary Material Fig. SM5 for samples 316-2 and -3), further extending those observed with small aliquots. Of the total number of aliquots that produced a natural signal of sufficient intensity, about half were excluded from the calculation of the average equivalent dose for reasons that are summarised in Table 2b. In the cases where the EBG subtraction procedure produced a significant increase in D_e, or where saturation effects (i.e., where $D_e>>2D_0$) were evident, the aliquots were also excluded. The latter are indicated by filled triangles in Fig. 10 for sample 316-1 and a radial plot of the values of PBG D_e for this sample is shown in Fig. 11a, together with a histogram (Fig. 11b) of the PBG D_e values used to calculate the weighted mean values when applying the selected statistical model (FMM, discussed below). A value of 15% overdispersion was combined in quadrature with the uncertainty associated with the equivalent dose measurement to account for the overdispersion observed in the dose recovery experiment. Equivalent plots of the data for samples 316-2 and -3 are shown in Supplementary Material Fig. SM6 (PBG D_e vs EBG D_e) and Fig. SM7 (radial and histogram plots of D_e).

FIGS. 9 & 10

The choice of statistical model applied to interpret the D_e distributions for the three samples was informed by the site formation model. The mechanism proposed in latter for the aggradation of sediment is the deposition of loess during cold stages, and subsequent reworking of loess with slope material, perhaps aided by the action of the seasonally thawed active layer, leading to the progressive infilling of the basin hollow. At the periphery of the hollow the reworking process is likely to have drawn into the mix a proportion of the underlying

sediment that had been deposited during the previous cold stage and under these conditions the sampled context would have contained a mixture of components, possibly including some partially bleached grains depending on the rate of the process. The FMM model was applied in the analysis of the D_e distributions to examine for the presence of resolved components. The relatively small number of D_e determinations place limitations on resolving D_e components within broad distributions using the model. Nonetheless, the application of the FMM (Galbraith, 2005), by seeking the maximum and minimum values respectively of the log likelihood and the Bayesian information criterion (BIC), produced two D_e components (k1 and k2, Table 2a, cols 12 and 13) for each of samples 316-1 (Fig. 11b, indicated by dotted lines) and 316-3 (Supplementary Material Fig. SM7b(ii)). It was not possible to resolve more than one component in the case of sample 316-2 and closer inspection of the SAR data indicates that this outcome may be associated with the distribution in the range of sensitivities (the signal recorded in response to the first monitor dose) of grains which, relative to the other two samples, shows a strong bias towards weaker emission. The two component values of D_e obtained for sample 316-1 (Table 2a, cols 12 and 13), 290±20 Gy (k1) and 560±40 Gy (k2), were calculated with an overdispersion of 4%; the model indicates that they are of roughly equal proportions. Similarly for sample 316-3, the two component values of D_e were 210±17 Gy (k1) and 295±55 Gy (k2) with an overdispersion of 7%; the dominant component is k1 although, with a RSE of 19%, k2 is less clearly resolved. After taking into account the dispersion evident in the dose recovery experiment, the overdispersion obtained by application of the mixture model appears to be consistent with a well bleached sediment. Although the overdispersion evaluated for sample 316-2 of 17% (in addition to the intrinsic 15% OD incorporated in the D_e uncertainty) is significantly larger than for the other two samples, it remains within the range that has been observed with well beached sediments (Olley et al., 2004 ; Galbraith et al., 2005; Bateman, 2007; Rowan et al., 2012), and the distribution of D_e values suggests that further testing may lead to the resolution of a second component >300 Gy. The weighted mean values of D_e determined for small aliquots (SA, 283±15 Gy) and very small aliquots (SG, 234±12 Gy) are expected to be similar if the grains have been drawn from

the same population. Comparison of the D_e histograms for small and very small aliquots suggests that inter-grain averaging has caused the distribution for small aliquots to be skewed towards higher dose values (histograms for VSA (8a) and SA (8c) data are given in Supplmentary Material Fig. SMA7). It is presumed that the finding that the width of the D_e distribution obtained with small aliquots was not significantly reduced by inter-grain averaging was partially due to the same, or similar, effect that caused the significant overdispersion observed in the dose recovery experiment. A variable level of contribution of the medium decay component is another potential source of overdispersion, but a significant contraction in the range of D_e values was not evident when the shorter integration interval of 200 ms was used in the EBG subtraction procedure.

FIG. 11

Given the significant additional instrument time required to perform a full sequence of SAR measurements with very small aliquots using this procedure, the dataset was considered to be sufficient to identify the primary features of the distribution(s). However, on the basis of the dose recovery experiments, the values of D_e above ca 400 Gy are likely to be underestimates of the absorbed dose and consequently the estimate for k2 of sample 316-1 should be considered to be a minimum dose, and if the mechanism causing an underestimation in the dose recovery experiment also applies to the evaluation of the natural dose, the average shortfall may amount to ~30%. It is interesting to note that in their study of Anglian Stage fluvial sediments, Pawley et al. (2010) were able to recover doses to 600 Gy with single aliquots (multiple grain), although underestimation was observed for higher levels of dose (600-800 Gy). In their study the EBG procedure was applied to obtain rigorous isolation of the fast component and the OSL signal intensity was sufficiently strong to avoid statistical fluctuation in the net signal obtained by EBG subtraction.

4. Dose rate

The total dose rate to coarse quartz grains, $\dot{D}_{tot}$, was assessed taking into account a) lithogenic sources emitting alpha and beta radiation located within the grains, and sources emitting beta and gamma radiation located within the medium external to the grains, and c) cosmic radiation. The external dose rates (Table 2d) were determined using the conventional measurement techniques of β TLD and high resolution γ spectrometry (Aitken, 1985). Several other methods, as discussed further below, were applied to obtain more detailed information regarding the distribution of radionuclides in the sediment.

The β-TLD technique used employs a single 10 mm diameter detector to measure the average β dose rate arising from sources distributed within the sample volume (~1 cm^3), and a calibration factor is applied to the measured dose rate to obtain the infinite medium dose rate (Aitken, 1985). The values of $D_{\beta+ig}$ shown in Table 2d (col. 2) for each sample represent the sum of the external beta dose rate, corrected for attenuation effects, and a small calculated contribution (0.03 mGy a^{-1}) to account for trace quantities of radionuclides within the grains (Table 2d, note 2).

The specific activities of ^{238}U, ^{232}Th and ^{40}K in the sediment samples (~25g) were measured using high resolution γ spectrometry. The values obtained (Table 2c) were used to calculate the infinite medium β and γ dose rates by applying conversion factors taken from Adamiec and Aitken (1998) for the ^{232}Th and $^{238}U/^{235}U$ series and from our own calculations for ^{40}K (Bailiff, 2007).

The ^{210}Pb: ^{226}Ra activity ratios obtained from the γ spectrometry measurements indicate longer term *in situ* loss of ^{222}Rn in the case of sample 316-1 (0.8±0.1; Table 2c, col. 5). However, the gamma dose rate for this location was calculated assuming secular equilibrium; if the current level of disequilibrium had been maintained throughout the burial period, the total dose rate predicted by calculation is expected to be ~2% lower (Aitken, 1985; Olley *et al.*, 1996).

The burial medium surrounding the three sampled contexts is predominantly composed of brickearth, apart from the thin sloping layer of flint pebbles (Fig. 2) between samples 316-1 and 316-2 which is at a sufficient distance from the samples to have a marginal effect on the gamma dose rate at both locations. The brickearth medium is structurally uniform and in calculating the contemporary gamma dose rate for each sampled location it was assumed that the radionuclide composition of the cored sample was representative of that contained in the surrounding 'γ' volume. A cosmic ray dose rate of 0.17±0.03 mGy a^{-1} was calculated (Prescott and Hutton, 1988; 1994) assuming an average overburden of 100 cm of sediment during the burial history of the sampled contexts and the combined γ and cosmic dose rate for each sample is given in Table 2d (col. 3). The measured values of moisture content in the sediment cores (Table 2d, col. 4) were used as the basis for arriving at an average value of 18±4 % for the burial period at all three locations. Although the site is in an upland position with an underlying Chalk geology, its location around a solution hollow would have resulted in cycles of relatively high moisture content in the sediment. Details of the other corrections to the dose rate are given in the notes to Table 2d.

4.1 Spatial variation of beta dose rate

Since estimates of the beta dose rate obtained using conventional techniques are averages for volumes much larger than the 'β' volume, an assessment of the potential for significant departures (Chauhan and Singhvi, 2011) from the assumed uniform dose rate for individual grains was investigated with sample 316-2. Measurements of the distribution of potassium, uranium and thorium were made to test whether the macroscopic structural uniformity of the brickearth observed visually reflected a uniform distribution of lithogenic radionuclides. In a separate study (Grainger, 2009) the distribution of K within the surface of a slice of resin-impregnated sediment was mapped using an SEM (with an EDXRF probe) and the technique of alpha autoradiography was applied using solid state nuclear track detectors (SSNTD; CR39, TASTRAK, Bristol, UK) to map the distribution of alpha emitting sources (U/Th). Elemental

analysis (ICP-MS and AAS) was also subsequently applied to the same slice to obtain the average concentrations of ^{238}U, ^{232}Th, ^{39}K and ^{91}Zr in ~20 mg samples obtained by drilling into the surface at six locations using a 1 mm dia. drill. The SEM elemental mapping of the sliced 316-2 sample confirmed a generally uniform distribution of potassium within the silt-sized components of the sediment and also a uniform distribution within the material of localised concentrations of potassium within diameters of ~100-120 μm, interpreted as coarse potassic feldspar grains. The alpha autoradiography maps for the same slice indicated a uniform distribution of alpha activity within the silt-sized components, but also extended clusters of activity (<100 μm) presumed to be associated with zircon grains on the basis of the detection of Zr in the drilled powder (ICP-MS). Of the ca 3700 tracks counted within the detector area (10 x 10 mm), less than 50 activity clusters were identified, indicating a relatively low concentration of U/Th bearing grains, and in subsequent elemental mapping (SEM) the presence of zircons was confirmed by examining a ~20 μm dia. grain exposed within the sample surface. The semi-quantitative estimates of the average concentrations (assuming equal activity) were 3.4 ppm U and 14.4 ppm Th obtained by track analysis, where the uncertainty has been estimated to be ±5% on the basis of work by Sanzelle et al. (1986). These values are broadly consistent with the average U and Th contents determined by gamma spectrometry (2.9±0.2(5) ppm U and 12.1±1.0 ppm Th). and by ICP-MS analysis of the drilled samples (3.4 ppm U and 12.4 ppm Th; analytical RSE, 2%; procedure tested with analysed stream sediment standard yielding central values for U and Th concentrations within 9% and 3% respectively of certified concentrations). However the variance was high (~38%) for both U and Th concentrations in the samples taken from six locations. Hence, overlying a generally uniform distribution of β emitters within the fine grained sample matrix, localised concentrations of K and U/Th in grain 'sources' (as indicated by SEM, ICP-MS and autoradiography) reveal the potential for non-uniformity in the beta dose rate on the scale of individual grains. Although the dose rate can be modelled for specified concentrations and spatial configurations of grain sources, the extent of spatial variation in the beta dose rate was

investigated experimentally by using a variant of the β-TLD technique that is at a developmental stage (Bailiff, 2012). The external β dose rate at the surface of a cut slice of resin encapsulated sample was measured with an array of up to 30 detectors. Each detector comprised Al_2O_3:C grains in a cylindrical cavity of ~1 mm dia. x 0.5 mm deep. Similar measurements were performed with a sample of ball-milled sediment from the same sampled core to provide the distribution for an ostensibly uniform matrix given previous reports of overdispersion in measured dose rates using Al_2O_3:C grains (Kalchgruber et al., 2003). The average dose rate for the resin impregnated sediment [1.18±0.03 μGy d^{-1} (s.e., n=31; RSD=15%)] is some 9% lower than that obtained with the powder [1.29±0.03 μGy d^{-1} (s.e., n=29; RSD 12%)]. A reduction in average dose rate and increased dispersion (Fig. 12) with a higher degree of heterogeneity is consistent with modelling simulations and calculations by Nathan et al. (2003) and Chauhan and Singhvi (2011). In both sets of results for 316-2 there is one outlying (higher) dose rate measurement that may be associated with a grain source and, if so, its presence in the powdered sample is surprising but may be the result of ball-milling that was insufficient to disperse smaller grains such as zircons of the size observed in the SEM examination. Although the relationship between the dispersion in the beta dose rate recorded using Al_2O_3:C grains in the geometry used here and that applying to individual quartz grains has yet to be determined, these distributions indicate an absence of significant non-uniformity in the beta dose rate.

FIG. 12

4.2 Effect of taphonomic processes

Following the initial deposition of sediment in the sampled contexts, changes in the composition of the sampled volume that affect the dose rate are potentially an important issue when interpreting the distribution of D_e values. The extent to which the sampled volume of sediment was an ‘open’ or ‘closed’ system to grains during the periods when the solution hollow was active and the effect of structural alterations during conditions of permafrost are unknown. However, the material present in the three sampled volumes appears to be

radiometrically similar in composition, with a difference in dose rate being some 12%, and the spatially resolved examination of sample 316-2 indicates a generally homogeneous medium. For the calculation of burial age discussed below the dose rate for the contemporary sampled environment has been assumed to represent the average dose rate for the burial period.

5. OSL ages and interpretation

The OSL burial ages were calculated using the weighted mean value of D_e obtained with very small aliquots and the average dose rate, $\dot{D}_{tot}$ (Table 2d, col. 5). The dose rate is given with two uncertainty terms, where the first is based on the calculated instrumental uncertainty in the beta and gamma dose rates and the second includes an uncertainty of ±10% assigned to both beta and gamma dose rates to account for the additional factors discussed above. The age calculated using the higher dose component of the D_e distribution (k2) for sample 316-1, 260±30 ka, should be regarded as a minimum burial age in view of the underestimation of D_e indicated by the outcome of the dose recovery experiment at high levels of dose.

It can be seen (Fig. 2b) that the OSL age for the sediment overlying the cobble layer containing the cultural material (316-2, 87±9 ka) and the OSL age for the most recent phase (k1) of the underlying sediment (316-1, 136±15 ka) place the deposition of this layer to between ca 90 and 140 ka ago. The similarity of the burial ages for 316-2 (87±9 ka) and 316-3 (75±9 ka) suggests that they may be associated with the same depositional event.

These OSL ages are clearly at odds with the Lower Palaeolithic assignment of the artefact assemblage. If the stratigraphic relationship between the horizons above and below the cobble layer deposits had been maintained despite a sub-aerial lowering of the land surface due to the solution process following the model at Wood Hall, and the sediments were uniformly bleached before burial, the OSL dates would be expected to be earlier and later than the age assigned typologically to the artefacts (>300 ka) for locations 316-1 and -2 respectively. Hence the significantly later OSL chronology for the emplacement of the cobble layer containing the artefacts suggests that the artefacts have not remained in a primary context. An alternative interpretation is that the OSL dates indicate hominin presence during the period 140-80 ka, but

there is no trace of Middle Palaeolithic material within the excavated artefact assemblage. While a hominin presence at West Cliffe during the last interglacial would have significant implications for the record of hominin occupation during that period (Lewis et al., 2011), the OSL dates indicate that that a more complex interpretation of the geological, archaeological and chronological data is required, the polycyclic site formation model for West Cliffe discussed earlier being one possible explanation. In this model sediment would have been reworked into the solution feature during interglacial periods when the solution process was active and the excavation provided evidence of the transfer of flint clasts and sediment via pipes (Sec. 2 and Fig. SM2). It is likely that during the onset of the last interglacial, following permafrost conditions, the flow of water was sufficient to disperse part of the pavement containing flint clasts and artefacts into the solution hollow, forming the cobble layer that was revealed by excavation, together with the cultural material. Consequently we conclude that the OSL ages place in time phases of reworking and reburial of sediments and associated artefact material within the solution hollow.

Given the various technical issues associated with the determination of D_e at high levels of dose, the number of grains with characteristics suitable for the determination of the initial burial age of the brickearth underlying the cobble layer is likely to be very small (requiring significant instrument time). However, with the aim of resolving the lower dose component(s) of the D_e distributions, further sampling of stratigraphically earlier and later deposits would enable a chronology for the reworking processes to be investigated in more detail.

6. Conclusion

By applying a novel experimental approach with very small aliquots of quartz grains of ~100 μm dia it has been possible to investigate the nature of significant overdispersion that had been observed in D_e values obtained using single aliquots containing multiple bright grains. These measurements revealed complexity of the luminescence characteristics of the quartz at high levels of dose (above ca 200 Gy). In particular, for grains that had received a known

laboratory dose in the dose recovery experiment, significant overdispersion in D_e and an underestimation of the applied dose, D_a, above ca 500 Gy were observed. Attempts to investigate whether changes in luminescence sensitivity during the measurement of the natural OSL accounted for the overdispersion, and potentially systematic underestimation of D_a at high dose, by monitoring the sensitivity of the 110 °C TL peak, indicate that if this were the case the latter does not appear to be a suitable proxy for OSL sensitivity. Similar dose recovery issues recently reported by Duller (2012) indicate that the effect is more widespread and further investigation is required.

The OSL scanning procedure can also be used more generally to determine the number of bright grains in small aliquots where resolution of components in the D_e distribution is of interest, where a single aliquot procedure is preferred (Rodnight et al., 2006; Reimann et al., 2012), and also to avoid problems arising from multiple grain occupancy of grain holes in a Risø single grain reader sample disc (Arnold et al., 2012). While the spatial variation in the beta dose rate did not appear to be a potential source of significant overdispersion in the equivalent dose for the West Cliffe samples, a better understanding of its extent on a sub-millimetre scale is required and this is likely to involve a combination of experimental dosimetry technique of the type discussed in this paper and further developments of autoradiographic techniques (Rufer and Preusser, 2009).

In analysing the D_e components of the three sediment samples, the OSL ages obtained for the burial of brickearth located stratigraphically below and above the clay and flint clast layer containing Lower Palaeolithic artefacts and debitage place the deposition of the artefacts in their excavated context to between ca 140 and 80 ka ago and this is significantly later than the Lower Palaeolithic typology assigned to the artefacts. We conclude that the cultural deposits were probably displaced from their primary context by processes associated with the development of the solution feature in which they occur and, given the timing of this process indicated by the OSL ages, the displacement may have occurred during the last interglacial

when the solution feature was active. This is contrary to expectation based on the study of other sites of similar age in the region such as Wood Hill. Although the extent of any artefact displacement is likely to vary according to specific conditions within the solution feature, the detection of reburial of the artefact assemblage is crucial to the interpretation of this and other sites where such processes may have occurred. At some sites, or parts of sites, there is evidence of *in situ* scatters that are only marginally affected by these disturbance processes or, if moved en masse, might survive, such as at Caddington where almost complete handaxe manufacturing sequences were reconstructed (Smith, 1894). However, we can no longer be confident about the timing of hominin use of the uplands in this area (White, 1997; Ashton et al., 2006), beyond broad statements of Lower or Middle Palaeolithic origin, or determine the environments that prevailed (White, 1997; Ashton et al., 2006; Campbell and Hubbard, 1978). Biological remains such as pollen or small vertebrates used to interpret the environment at the time of occupation would consequently date, not to the period of original artefact discard, but to one or more subsequent periods of reworking. Although most of the currently-known 'doline' sites in south Britain are devoid of well-preserved organic remains, reconstruction of the environment at the time of hominin occupation remains problematic. A better knowledge of the archaeology of these upland landscapes is essential if a fuller understanding of the record of hominin occupation beyond the river valleys is to be achieved. The study described in this paper has demonstrated the potential of luminescence techniques to date sediments associated with karst landscapes and also that caution is required when interpreting the archaeological signatures from upland sites on Chalk bedrock. Where possible, both burnt flint and burial horizon should be tested using luminescence and further developments of this approach, together with renewed field investigation, may help to refine the chronology of landscape development in such upland areas, particularly if deposits more deeply buried in solution hollows can be recovered and dated.

Acknowledgements

IKB thanks Scott Grainger for laboratory technical support and Dr Rex Galbraith for access to his equivalent dose modelling code. Prof. Geoff Duller and Dr Andrew Millard are thanked for their helpful comments on draft versions of the paper. HCD and MJW thank Geoff Halliwell and the Dover Archaeological Group for access to the site and collections, Dr Beccy Scott and the excavation team, including Andy Shaw, Tom White, Dave Underhill, Rob Dinnis and Ed Cork. SL acknowledges the support of the Ancient Human Occupation of Britain Project funded by the Leverhulme Trust.

References

Adamiec, G., 2005. OSL decay curves – relationship between single- and multiple- grain aliquots. Radiation Measurements 39, 63-75.

Adamiec, G., Aitken, M.J., 1998. Dose rate conversion factors: update. Ancient TL 16, 37-50.

Aitken, M.J., 1985. Thermoluminescence Dating. Academic Press, London.

Aitken, M.J., 1998. An introduction to optical dating. Oxford University Press, Oxford.

Arnold, L.J., Roberts, R.G., Galbraith, R.F., DeLong, S.B., 2009. A revised burial dose estimation procedure for optical dating of young and modern-age sediments. Quaternary Geochronology 4, 306-325.

Arnold, L.J., Demuro, M., Navazo Ruiz, M., 2012. Empirical insights into multi-grain averaging effects from 'pseudo' single-grain OSL measurements. Radiation Measurements 47, 652-658

Ashton, N., Lewis, S. G; Parfitt, S., White, M., 2006. Riparian Landscapes and Human Habitat Preferences During Hoxnian (MIS 11) Interglacial. J. Quaternary Science 21 (5), 497-505.

Bailey, R.M., 2001. Towards a general kinetic model for optically and thermally stimulated luminescence of quartz. Radiation Measurements 33 17-45.

Bailiff, I.K., 2007. Methodological developments in the dating of brick from late medieval and post medieval English buildings. Archaeometry 49, 827-851.

Bailiff, I.K., 2012. Spatially resolved measurement of beta dose rate using external dosemeters. Abstract. 13th International Conference on Luminescence and Electron Spin resonance Dating, 10-14 July 2011, Toruń, Poland.

Bailiff, I.K., Mikhailik, V., 2003. Spatially resolved measurement of optically stimulated luminescence and time-resolved luminescence. Radiation Measurements 37, 151-159.

Ballarini, M., Wallinga, J., Wintle, A.G., Bos, A.J.J., 2007. A modified SAR protocol for optical dating of individual grains from young quartz samples. Radiation Measurements 42, 360-369.

Barreto, H., Howland, F.M., 2006. Introductory Econometrics, Cambridge University Press, Cambridge, UK.

Bateman, M.D., Boulter, C.H., Carr, A.S., Frederick, C.D., Peter, D., Wilder, M., 2007. Detecting post-depositional sediment disturbance in sandy deposits using optical luminescence. Quaternary Geochronology 2, 57-64.

Berger, G.W., 1990. Regression and error analysis for a saturating-exponential-plus-linear model. Ancient TL 8, 23-25.

Bourguignon L., Blaser J., Rios L., Pradet L., Sellami F., Guibert P., 2008. L'occupation moustérienne de la Doline de Cantalouette II (Creysse, Dordogne) : spécificités technologiques et économiques, premiers résultats d'une analyse intégrée, Bulletin de la Société Préhistorique Française XLVII, 133-150.

Brennan, B. J., 2003. Beta doses to spherical grains. Radiation Measurements, 37**,** 299-303.

Bridgland, D. R., 1994. Quaternary of the Thames. Geological Conservation Review Series. Chapman and Hall. London.

Bulur, E., 2000. A simple transformation for converting CW-OSL curves to LM-OSL curves. Radiation Measurements 32, 141-145.

Campbell, J. B., Hubbard, R. N. L., 1978. Biological investigation of the Rackley Site. In*:* Sampson, C. G. (ed.) Paleoecology and archaeology of an Acheulian site at Caddington, England. Dallas: Southern Methodist University. 47-60.

Chauhan, N., Singhvi, A.K., 2011. Distribution of SAR palaeodoses due to spatial heterogeneity of natural beta dose. Geochronometria 38, 190-198.

Cunningham, A.C., Wallinga, J., 2010. Selection of integration time intervals for quartz OSL decay curves. Quaternary Geochronology 5, 657-666.

Cunningham, A.C., Wallinga, J., Minderhoud, P.S.J., 2011. Expectations of scatter in equivalent dose distributions when using multi-grain aliquots for OSL dating. Geochronometria 38, 414-431.

Diez-Martín, F., Sánchez-Yustos, P., Gómez-González, J. Á., Gómez de la Rúa, D., 2008. Earlier Palaeolithic Settlement Patterns: Landscape Archaeology on the River Duero Basin Plateaus (Castilla y León, Spain) J World Prehist. 21,103–137.

Drinkall, H. C., 2005. Elevated Hominids: the dating feasibility and Palaeolithic assemblage from the site of West Cliffe Saint Margaret, Dover, Kent. Unpublished MA thesis. Department of Archaeology, Durham University.

Duller, G.A.T., 2008. Single-grain optical dating of Quaternary sediments: why aliquot size matters in luminescence dating. Boreas 27, 589-612.

Duller, G.A.T., 2012. Improving the accuracy and precision of equivalent doses determined using the optically stimulated luminescence signal from single grains of quartz. Radiation Measurements 47, 770-777.

Durcan, J., Duller, G.A.T., 2011. The fast ratio: a rapid measure for testing the dominance of the fast component in the initial OSL signal from quartz. Radiation Measurements 46, 1065-1072.

Ford, D., Williams, P., 1989. Karst Geomorphology and Hydrology. Chapman and Hall. London.

Galbraith, R.F., 2005. Statistics for Fission Track Analysis. Chapman and Hall/CRC Press, Boca Raton, Florida.

Galbraith, R.F., Roberts, R.G., Yoshida, H., 2005. Error variation in OSL palaeodose estimates from single aliquots of quartz: a factorial experiment. Radiation Measurements 39, 289 – 307.

Galbraith, R.F., Roberts, R.G., 2012. Statistical aspects of equivalent dose and error calculation and display in OSL dating: an overview and some recommendations. Quaternary Geochronology 11, 1-27.

Göksu, H.Y., Bailiff, I.K., Bøtter-Jensen, L., Hütt, G., Stoneham, D., 1995. Inter-laboratory beta source calibration using TL and OSL with natural quartz. Radiation Measurements 24, 479-484.

Grainger, S., 2009. Development of techniques for high-resolution spatially-resolved elemental analysis in materials of interest in luminescence dating. Unpublished MSc thesis, Durham University.

Guibert, P., Bechtel, F., Bourguignon, L., Brenet, M., Couchoud, I., Delagnes, A., Delpech, F., Detrain, L, Duttine, M, Folgado, M., Jaubert, J., Lahaye, C., Lenoir, M., Maureille, B., Texier, J-P., Turq, A., Viellevigne, E., Villeneuve, G., 2008. Une base de données pour la chronologie du Paléolithique moyen dans le Soud-Ouest de la France. Memoire de la Société Préhistorique Française XVVII, 19-40.

Halliwell, G., Parfitt, K., 1993. Non-River Gravel Lower and Middle Palaeolithic Discoveries in East Kent. Kent Archaeological Review 114, 80-89.

Jacobs, Z., Roberts, R.G., Nespoulet, R., El Hajraoui, M.A., Debénath, A., 2012. Single-grain OSL chronologies for Middle Palaeolithic deposits at El Mnasra and El Harhoura 2, Morocco: Implications for Late Pleistocene human environment interactions along the Atlantic coast of northwest Africa. J. Human Evolution 62, 377-394.

Jain, M., Murray, A.S., Bøtter-Jensen, L., 2003. Characterisation of blue-light stimulated luminescence components in different quartz samples: implications for dose measurement. Radiation Measurements 37, 441-449.

Jennings, J. N., 1985. Karst geomorphology. Blackwell, Oxford.

Kalchgruber, R., Fuchs, M., Murray, A.S., Wagner, G.A., 2003. Evaluating dose-rate distributions in natural sediments using α-Al_2O_3:C grains, Radiation Measurements 37, 293-297.

Lewis, S.G., Ashton, N.M., Jacobi, R.M., 2011. Testing human presence during the Last Interglacial (MIS 5e): a review of the British evidence. In: Ashton, N., Lewis, S.G., Stringer, C.B. (Eds). *The Ancient Human Occupation of Britain*. Developments in Quaternary Science, 14. Elsevier, Amsterdam, 125-164.

Li, B., Li, S-H., 2006. Comparison of D_e estimates using the fast component and the medium component of quartz OSL. Radiation Measurements 41, 125-136.

Loveday, J.,1962. Plateau deposits of the southern Chiltern Hills, Proceedings of the Geologists' Association 73, 83-102.

Murray, A.S., Wintle, A.G., 2000. Luminescence dating of quartz using an improved single-aliquot regenerative-dose protocol. Radiation Measurements 32, 57-73.

Murray, A.S., Wintle, A.G., 2003. The single-aliquot regenerative–dose protocol: potential for improvement. Radiation Measurements 37, 377-381.

Murray, A.S., Buylaert, J.-P. Henriksen, M., Svendsen, J.-I., Mangerud, J., 2008. Testing the reliability of quartz OSL ages beyond the Eemian. Radiation Measurements 43, 776–780.

Nathan. R.P., Thomas, P.J., Jain, M., Murray, A.S., Rhodes, E.J., 2003. Environmental dose rate heterogeneity of beta radiation and its implications for luminescence dating: Monte Carlo modelling and experimental validation. Radiation Measurements 37, 305-313.

Olley, J.M., Murray, A., Roberts, R.G., 1996. The effects of disequilibria in the uranium and thorium decay chains on burial dose rates in fluvial sediments. Quaternary Science Reviews (Quaternary Geochronology) 15, 751-760.

Olley, J.M., Pietsch, T., Roberts, R.G., 2004. Optical dating of Holocene sediments from a variety of geomorphic settings using single grains of quartz. Geomorphology 60, 337-358.

Parfitt, K., Halliwell, G. 1996. More Palaeolithic Discoveries in East Kent. Kent Archaeological Review 123, 58-64.

Pawley S.M., Toms, P., Armitage, S.J., Rose, J., 2010. Quartz luminescence dating of Anglian Stage (MIS 12) fluvial sediments: Comparison of SAR age estimates to the terrace chronology of the Middle Thames valley, UK. Quaternary Geochronology 5, 569-582.

Prescott, J.R., Hutton, J.T., 1988. Cosmic ray and gamma ray dosimetry for TL and ESR. Radiation Measurements 14, 223-227.

Prescott J.R., Hutton J.T.,1994. Cosmic ray contribution to dose rates for luminescence and ESR dating: large depths and long-term time variations. Radiation Measurements 23, 497-500.

Reimann, T., Lindhost, S., Thomsen, K.J., Murray, A.S., Frechen, M., 2012. OSL dating of mixed coastal sediment (Sylt, German bright, North Sea). Quaternary Geochronology, in press.

Rodnight, H., Duller, G.A.T., Wintle, A.G., Tooth, S., 2006. Assessing the reproducibility and accuracy of optical dating of fluvial deposits. Quaternary Geochronology 1, 109-120.

Rowan, A.V., Roberts, H.M., Jones, M.A., Duller, G.A.T., Covey-Crump, S.J., Brocklehurst, S.H., 2012. Optically stimulated luminescence dating of glaciofluvial sediments on the Canterbury Plains, South Island, New Zealand. Quaternary Geochronology 8, 10-22.

Rufer, D., Preusser, F., 2009. Potential of autoradiography to detect spatially resolved radiation patterns in the context of trapped charge dating. Geochronometria 34, 1-13.

Sampson, C. G., 1978. Palaeolecology and Archaeology of an Acheulian Site at Caddington, England. Dallas: Southern Methodist University.

Sanzelle, S., Fain J., Mailler, D., 1986. Theoretical and experimental study of alpha counting efficiency using LR-115 Kodak SSTND applied to dosimetry in the field of thermoluminescence dating. International Journal of Radiation Applications and Instrumentation. Part D. Nuclear Tracks and Radiation Measurements 12, 913 916.

Schreve, D.C., 2001. Differentiation of the British late middle Pleistocene interglacials: the evidence from mammalian biostratigraphy. Quaternary Science Reviews 20, 1693–1705.

Scott-Jackson, J. E., 2000. Lower and Middle Palaeolithic artefacts from deposits mapped as Clay-with-Flints: A new synthesis with significant implications for the earliest occupation for Britain. Oxbow Books. Oxford.

Scott-Jackson, J. E., Walkington, H. , 2005. Methodological issues raised by laser particle size analysis of deposits mapped as Clay-with-flints from the Palaeolithic site of Dickett's Field, Yarnhams Farm, Hampshire, UK. J. Archaeological Science 32, 969-980.

Singhvi, A.K., Stokes, S.C., Chauhan, N., Nagar, Y.C., Jaiswal, M.K., 2011. Changes in natural OSL during single aliquot regeneration procedure and their implications for equivalent dose determination. Geochronometria 38, 231-241.

Singarayer, J.S., Bailey, R.M., 2003. Further investigations of the quartz optically stimulated luminescence components using linear modulation. Radiation Measurements 37, 451-458.

Smith, W. G., 1916. Notes of the Palaeolithic floor near Caddington. Archaeologia 67, 49-74.

Steffen, D., Preusser, F., Schlunegger, F., 2009. OSL quartz age underestimation due to unstable signal components. Quaternary Geochronology 4, 353-362.

Torri, D., Sfalanga, M; G. Chisci., 1987. Threshold conditions for incipient rilling. In Bryan, R. B. (ed). Rill Erosion, Processes and Significance. Catena Supplement 8. 97-105.

Tuffreau, A., Maotte, A., Goval, E., 2008. Les industries acheuléennes de la France septentrionale. L'Anthropologie 112, 104-139.

Waltham, T., Bell, F., Culshaw, M., 2005. Sinkholes and Subsidence, Karst and Cavernous Rocks in Engineering and Construction. Praxis Publishing, UK.

White, M. J., 1997. The earlier Palaeolithic occupation of the Chilterns (southern England): re-assessing the sites of Worthington G. Smith. Antiquity 71**,** 912-31.

Wintle A.G., 1973. Anomalous fading of thermoluminescence in mineral samples. Nature 245, 143-144.

Wintle, A.G., Murray, A.S., 2006. A review of quartz optically stimulated luminescence characteristics and their relevance in single-aliquot regeneration dating protocols. Radiation Measurements 41, 369-391.

Zimmerman, D.W., 1971. Thermoluminescent dating using fine grains from pottery. Archaeometry 13, 29-52.

Tables

Table 1. OSL single aliquot regenerative procedure

Step	Procedure	Measurement
1	PH1; OSL	Pre-heat using a selected temp. within the range 240-280 °C; measure OSL
2	PH2; OSL	Pre-heat monitor (PHM)
3	ß1; PH1; OSL	1st dose point / Sensitivity Monitor
4	PH2; OSL	PHM
5	ß2; PH1; OSL	2nd dose point
6	PH2; OSL	PHM
7-18		Repeat Steps 3-6 with 3rd, 4th and 5th dose points.
19	β9; PH1; OSL	Repeat ß2/Recycling test
20	PH2; OSL	PHM
21	β10; PH1; IRSL; OSL	Test for IR depletion
22	PH2; OSL	PHM

Notes

1. The OSL decay curve was measured for 20s with the sample temperature held at 125 °C during stimulation.
2. The preheat PH1 was performed by heating the aliquot (5 ˚C s^{-1}) to a maximum temperature selected in the range 240-280 ˚C, recording the TL, holding at the maximum temperature for 5s, cooling to RT and then repeating the procedure. The preheat PH2 was performed by heating once to the maximum temperature as in PH1 and holding at that temperature for 10s.
3. ßn represents the administration of a laboratory ß dose in the regenerative sequence, where n=1, 3, 5 and 7 corresponds to the monitor dose, n=9 repeats ß2, and where n= 2, 4, 6 and 8 corresponds to multiples of 0.75, 1.5, 2.25 and 3 of the monitor dose. The monitor dose was typically 200 Gy.
4. In the dose recovery experiment the beta dose D_α was applied following optical blceaching with blue LEDs before step 1, as described in the main text.

Table 2a. Analysis of D_e values: very small aliquots

	Single aliquot			Dose Recovery				Model		Equivalent dose, burlal Single Grain		
Sample	D_e CDM (Gy)	OD (%)	n	D_a (Gy)	D_e CDM (Gy)	OD (%)	n		OD (%)	n	D_e k 1 (Gy)	D_e k2 (Gy)
316-1	355±15	13	10	205 408 612	233±8 380±13 450±24	13 0 9	19 4 4	CDM FMM	36 4[1]	18	290±20 [55±13%]	560±40 [45±13%]
316-2	283±15	26	24	213	218±10	17	19	CDM	17[1]	26	234±12	
316-3	215±17	21	8	208	219±9	12	10	CDM FMM	22 7[1]	20	210±17 [74±26%]	295±55 [26±26%]

Notes

1. In addition to 15% overdispersion parameter (σ_B) combined in quadrature to account for intrinsic effects based on the dose recovery analysis.
2. OD, overdispersion; CDM, central dose model; FMM, finite mixtures model; n, number of determinations.

Table 2b. Aliquot testing statistics

		Number of excluded aliquots								
Sample	Tested	DC change	Scatter	Satn	$I>I_{sat}$	Scan	3gr	2gr	D_e change EBG	Accepted VSA 1gr
316-1	42	1	5	2	1	1	1	9	4	18
316-2	48	4	7	2	2	-	3	2	2	26
316-3	33	3	3	1	-	-	2	4	-	20

Notes

1. The total number of aliquots that produced OSL of adequate intensity is indicated in col. 2 and the number of aliquots accepted for the calculation of the weighted mean value of D_e in col. 11.
2. The causes of exclusion of aliquots are indicated in the intervening cols: DC change, change in form of decay curve from step 1 to step 3 (Table 1); Satn, $D_e >> 2D_o$; Scatter, significant statistical fluctuation in OSL signals or data points in the growth characteristic; $I_N>I_{sat}$; natural OSL signal did not intersect with the dose response curve, lying above the projected asymptotic saturation value; Scan, individual grains not resolved in scan data; 3gr and 2gr, OSL dominated by three and two grains in aliquot respectively; D_e changes, significant difference between EBG D_e and PBG D_e as discussed in main text.

Table 2c. γ spectrometry data

Sample	Th (Bq kg^{-1})	U (Bq kg^{-1})	K (Bq kg^{-1})	Ratio $^{210}Pb/^{226}Ra$
316-1	44.9±3.1	22.5±1.7	354±6	0.8±0.1
316-2	49.2±3.3	37.1±1.9	434±7	0.9±0.1
316-3	44.4±3.2	38.2±1.9	434±7	1.0±0.1

Table 2d. OSL ages and related data

Sample	$\dot{D}_{\beta+\square ig}$ (mGy a^{-1})	$\dot{D}_{\gamma+\square cos}$ (mGy a^{-1})	H_2O %	$\dot{D}_{tot}$ (mGy a^{-1})	D_e (Gy)	VSA SG OSL Age (ka)
316-1	1.15	0.99	18	2.14 ±0.05; ±0.14	290±20 (k1) 560±40 (k2)	136±15 260±30
316-2	1.49	1.20	18	2.69 ±0.06; ±0.18	234±12	87±9
316-3	1.65	1.16	14	2.81 ±0.06; ±0.19	210±17 (k1) 295±55 (k2)	75±9 105±22

Notes

1. The values of the point absorber beta dose rate within the tested material, obtained using β-TLD, were reduced (by 5% for 75-90 μm grains) to account for the effects of attenuation due to the finite size of the quartz grains using our calculations that are similar to those published by Brennan (2003).
2. An allowance of 0.03 mGy a^{-1} was made for the internal grain dose rate (alpha and beta) arising from radionuclides within the quartz and based on a measured average value in quartz.
3. The gamma dose rate at each location was calculated using the average measured radionuclide concentrations in the sediment sample and applying conversion factors based on those given by Adamiec and Aitken (1998) and our own calculations.
4. Corrections for moisture content (assumed to be 18±4% for contexts) were applied to both beta and gamma dose rates using factors (ratio of absorption coefficients for water and ceramic) of 1.25 and 1.14 for the beta and gamma dose-rates respectively, as calculated by Zimmerman (1971).
5. The cosmic dose rate was calculated (Prescott and Hutton, 1988; 1994) assuming an average overburden of 160 g cm^{-2} during burial.
6. The total dose rate (col. 5) is given with two uncertainty terms; the first is the calculated instrumental error and the second includes an increased uncertainty of ±10% assigned to the beta and gamma dose rates as discussed in the main text.
7. The reference date for age calculation is 2010.

Figure Captions

Figure 1.

Isometric view of chalk surface of the Westcliffe site, created in ArcGIS and extrapolated from the borehole data. The boreholes are marked as dots and the main excavation, Area 1, is filled in black. Lighter areas on the surface representation are relatively higher points and darker areas are relatively lower. The labels A-C identify the three solution features discussed in the main text.

Figure 2

a) Plan of Area 1, showing location of main excavations, position of sections 04/1-4 and the main artefact concentration within the trench;

b) Section 04/04 through the cobble layer and positions of OSL core samples.

Figure 3.

Isometric 3D plot of the spatially resolved OSL intensity recorded with an aliquot of quartz grains located on the measurement disc located in the x-y plane. The sharp peak in the plot represents the emission from a dominant individual bright grain and for this peak the ratio of signal to background was 4:1. The OSL is recorded at 1600 measurement points within the scanned area (10 x 10 mm).

Figure 4.

OSL decay curve measured with an aliquot of sample 316-1 and recorded with a counter interval of 10 ms. Three OSL decay components were fitted to the decay curve using a non-linear least squares fitting algorithm, indicating the presence of fast, medium and slow decay components with values of the decay constant, b (s^{-1}), of 1.90, 0.46 and 0.02 respectively. For a signal integration interval of 0-800 ms the medium decay component contrubutes 7% of the total signal.

Figure 5.

Dose response characteristics measured with single aliquots of sample 316-2: a) D_e vs D_0 and b) D_e vs EBG D_e. The signal and background integration intervals were both 0-800 ms in the case of PBG subtraction and 0-800 ms and 800-1600 ms for EBG subtraction respectively. The dashed lines correspond to: a) the limit of the recommended working dose range, $D_e=2D_0$ and b) ±20% of equivalence (dash-dot); the open data symbols indicate values of D_e exceeding $2D_0$.

Figure 6.
Dose recovery experiment: comparison of D_e values obtained for very small aliquots, each containing a dominant individual bright grain, using the PBG and EBG subtraction procedures, shown for sample 316-1. The applied dose, D_a, is indicated by the dashed lines drawn parallel to each axis; with zero overdispersion the D_e values are expected to lie close to the point of intersection.

Figure 7.
Dose recovery experiment: a) comparison of D_e values obtained for very small aliquots of sample 316-1, each containing a dominant individual bright grain, using the PBG and EBG subtraction procedures as shown in Fig. 6, together with D_e values obtained for two higher levels of applied dose (D_a =408 and 612 Gy), and b) the data shown in a) plotted against D_a.

Figure 8.
Dose recovery experiment: comparison of D_e values obtained for very small aliquots of sample 316-1, each containing a dominant individual bright grain, using the PBG subtraction procedure as shown in Fig. 6, but where the first OSL signal (Step 1, Table 1, following administration of the applied dose) is corrected for change in sensitivity as discussed in the main text. The applied dose, D_a, is indicated by the dashed lines drawn parallel to each axis; with zero overdispersion the D_e values are expected to lie close to the point of intersection (205 Gy). The data points shown as open symbols are discussed in the main text.

Figure 9.
Dose response characteristic measured with very small aliquots, each containing a dominant individual bright grain. The plot of D_e vs D_0 is shown for sample 316-1 where the dashed line corresponds to the limit of the recommended working dose range, $D_e=2D_0$.

Figure 10.
Dose response characteristic (PBG D_e vs EBG D_e) measured with very small aliquots from sample 316-1, each containing a dominant individual bright grain. The signal and background integration intervals were both 0-800 ms in the case of PBG subtraction and 0-800 ms and 800-1600 ms for EBG subtraction respectively. The filled triangle data symbols indicate exclusion from the calculation of the average D_e (see main text). The dashed lines correspond to ±20% of equivalence (dash-dot).

Figure 11.

Histogram (i) and radial plot (ii) of PBG D_e values shown in Fig. 10 that were used to calculate the weighted average for very small aliquots from sample 316-1, each containing a dominant individual bright grain. The broken lines indicate the value of the D_e components evaluated using the FMM model.

Figure 12.
Histogram of values of external beta dose rate measured using spatially resolved βTLD with a sample of 316-2 in powder form (upper) and impregnated with resin (lower). The background dose rate has been subtracted.

Fig.1

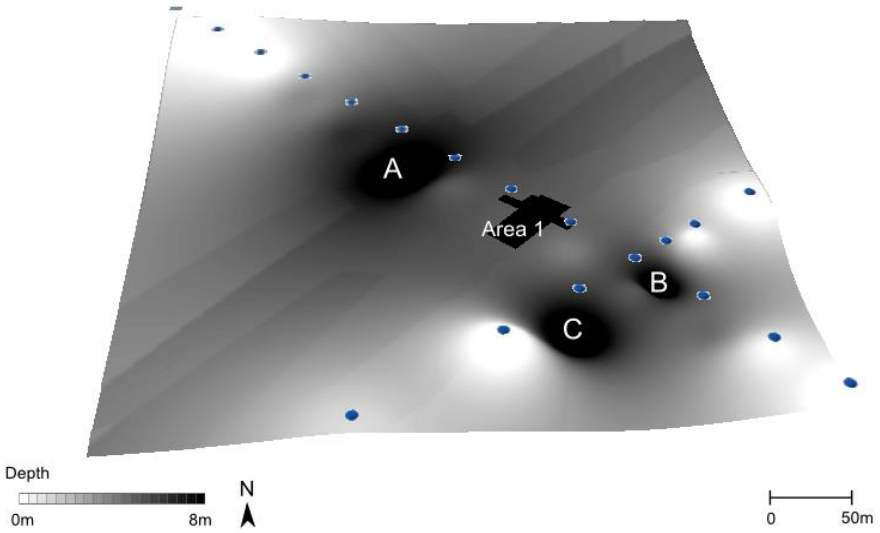

Fig. 2

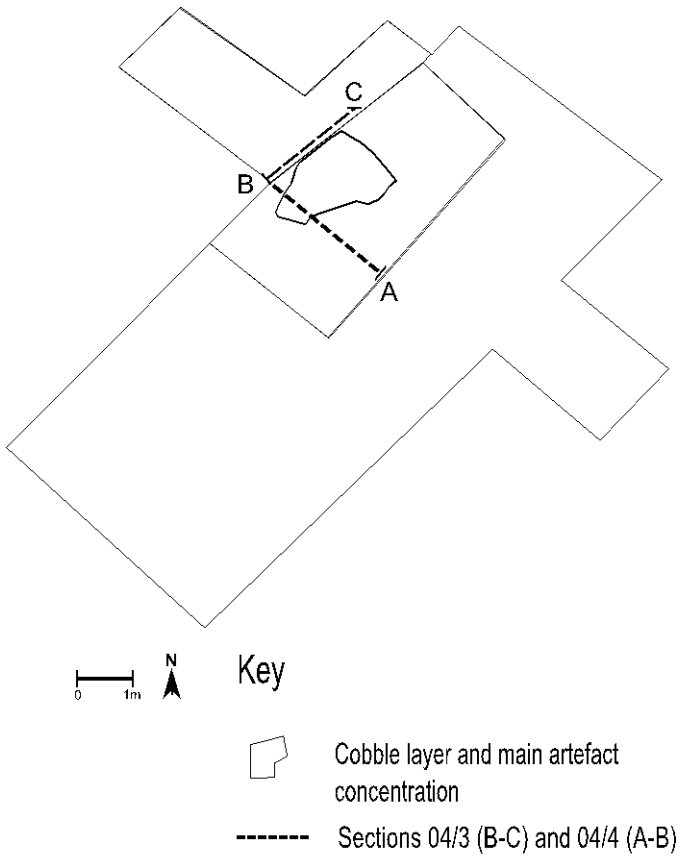
C
B
A
0
1m
N
Key
Cobble layer and main artefact concentration
Sections 04/3 (B-C) and 04/4 (A-B)

a)

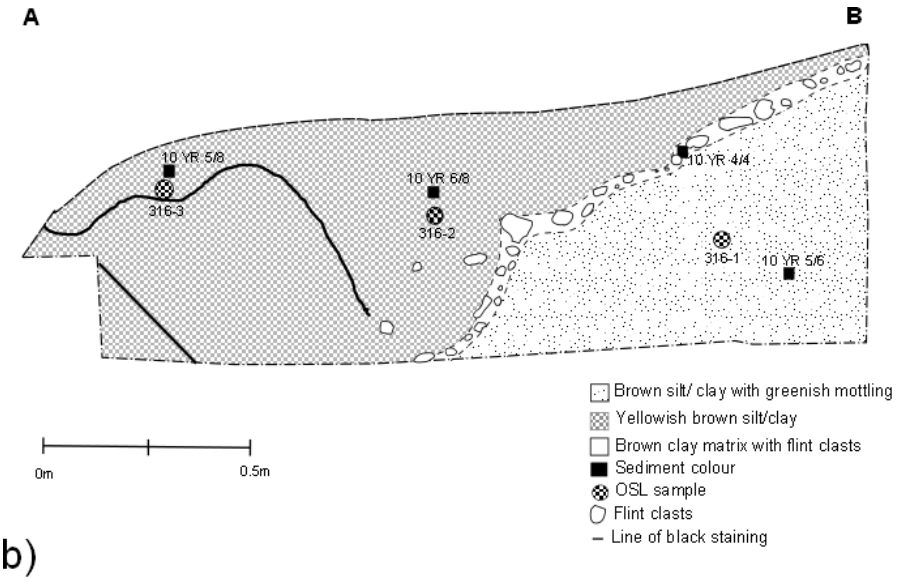
A
B
10 YR 5/8
316-3
10 YR 6/8
316-2
10 YR 4/4
316-1
10 YR 5/6
0m
0.5m
Brown silt/ clay with greenish mottling
Yellowish brown silt/clay
Brown clay matrix with flint clasts
Sediment colour
OSL sample
Flint clasts
Line of black staining

b)

Fig. 3

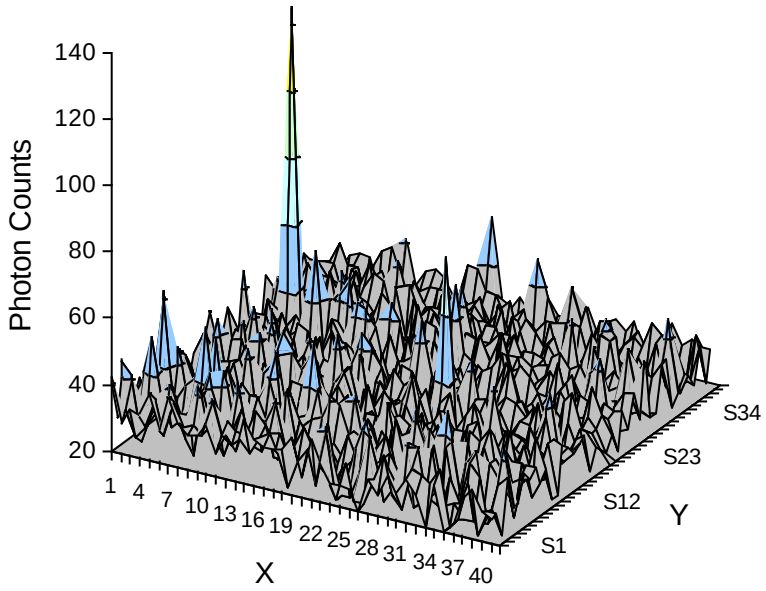
Photon Counts
140
120
100
80
60
40
20
1 4 7 10 13 16 19 22 25 28 31 34 37 40
X
S1
S12
S23
S34
Y

Fig. 4

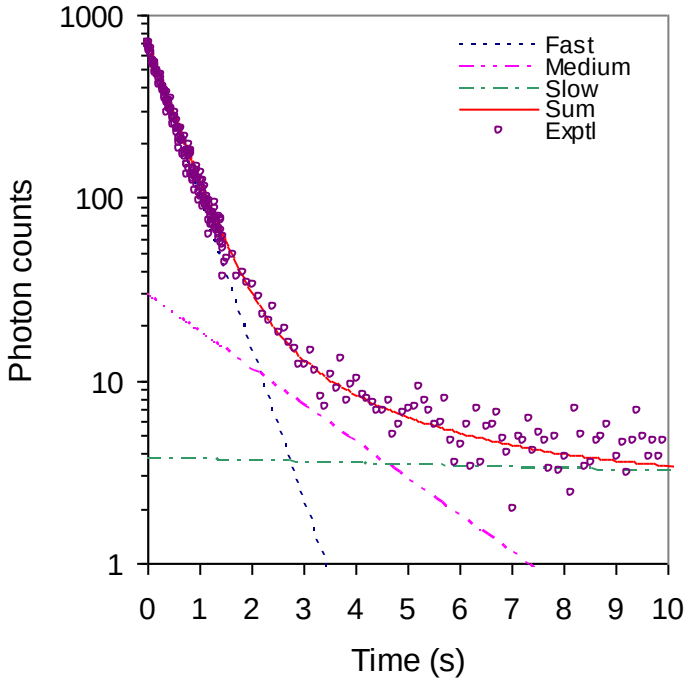
1000
100
10
1
Photon counts
0
1
2
3
4
5
6
7
8
9
10
Time (s)
Fast
Medium
Slow
Sum
Exptl

Fig. 5

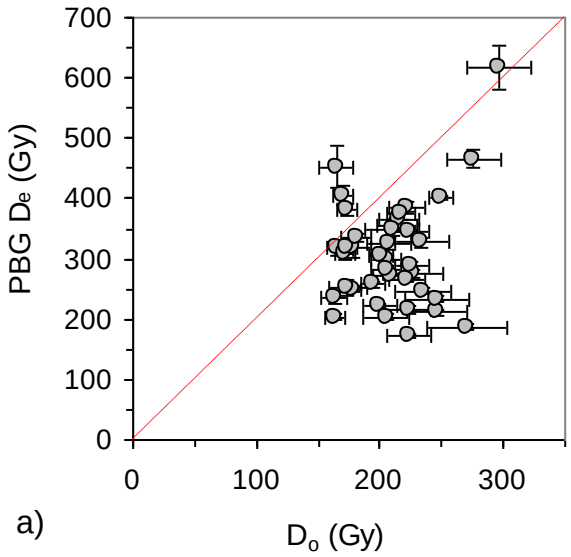
700
600
500
400
300
200
100
0
PBG De (Gy)
0
100
200
300
Do (Gy)

a)

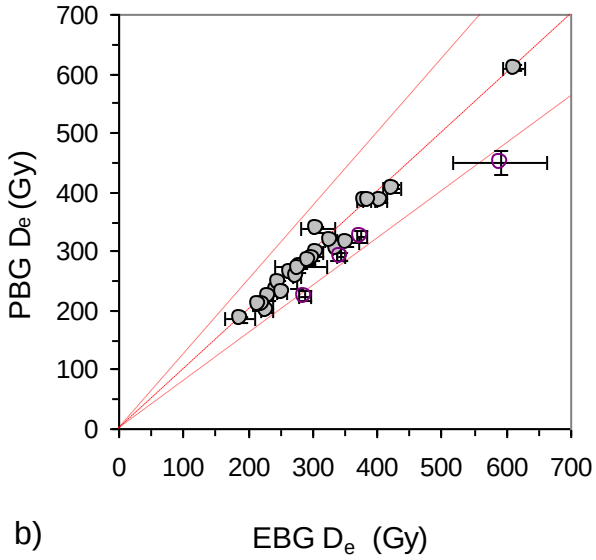
700
600
500
400
300
200
100
0
PBG De (Gy)
0
100
200
300
400
500
600
700
EBG De (Gy)

b)

Fig. 6

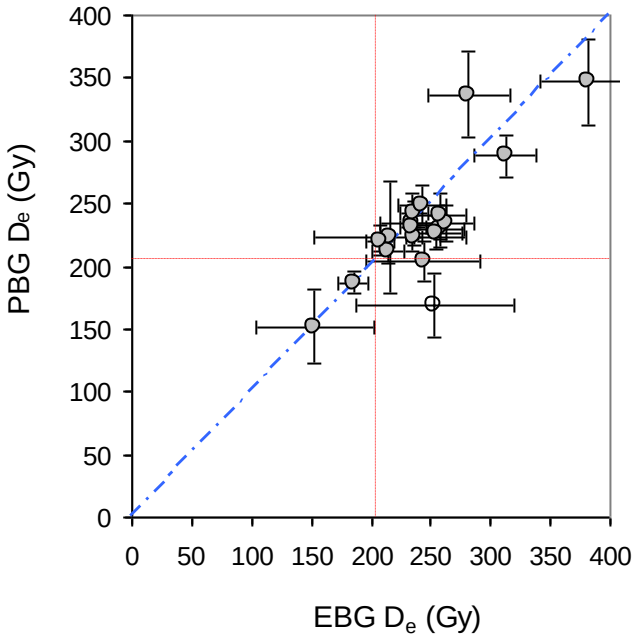
400
350
300
250
200
150
100
50
0
PBG De (Gy)
0
50
100
150
200
250
300
350
400
EBG De (Gy)

Fig. 7

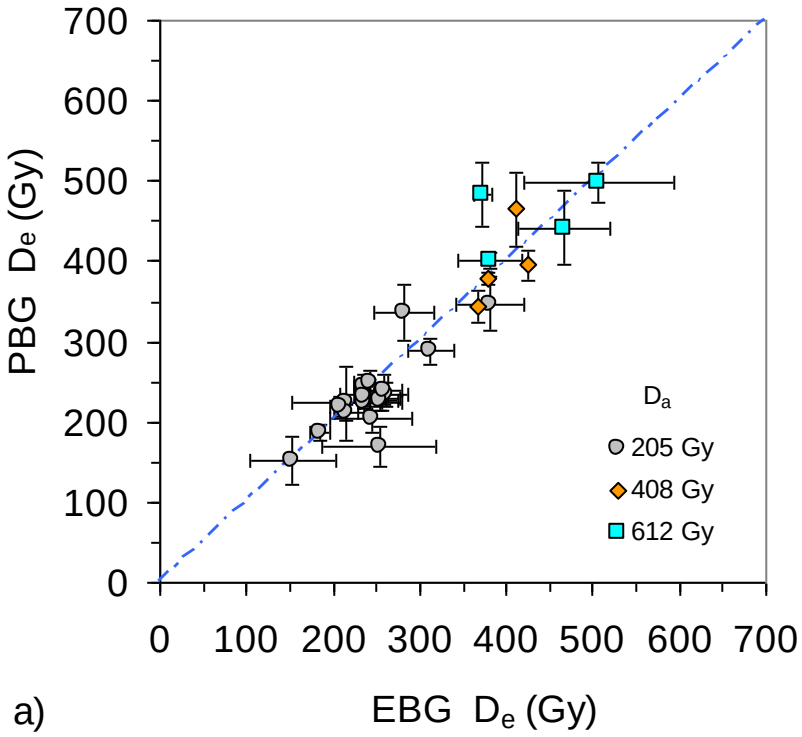
700
600
500
400
300
200
100
0
PBG De (Gy)
0 100 200 300 400 500 600 700
EBG De (Gy)
Da
205 Gy
408 Gy
612 Gy

a)

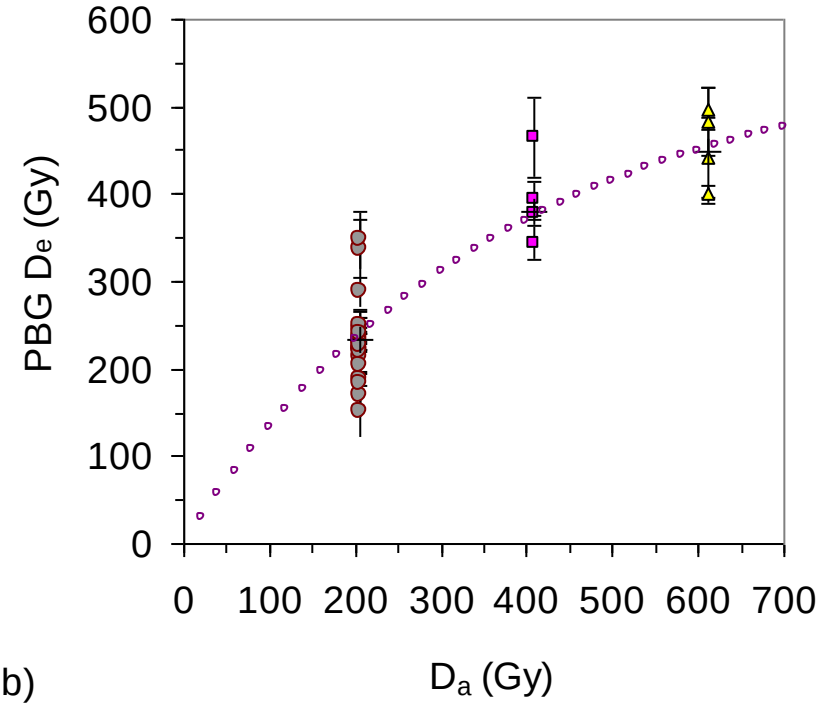
600
500
400
300
200
100
0
PBG De (Gy)
0 100 200 300 400 500 600 700
Da (Gy)

b)

Fig. 8

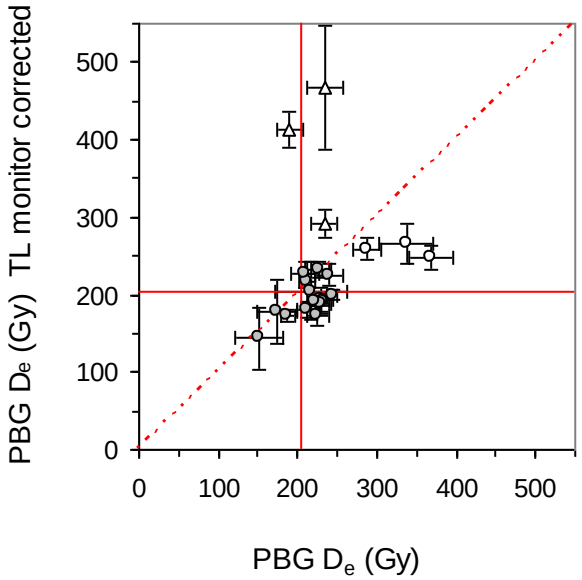
PBG De (Gy) TL monitor corrected
PBG De (Gy)
0
100
200
300
400
500

Fig. 9

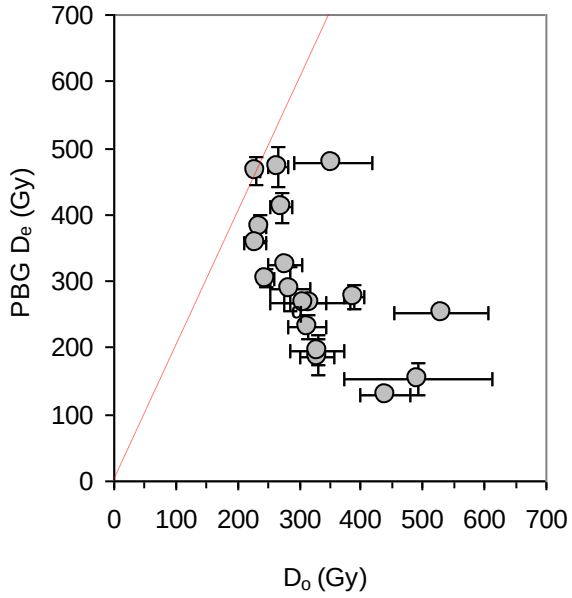
PBG De (Gy)
Do (Gy)
0
100
200
300
400
500
600
700

Fig. 10

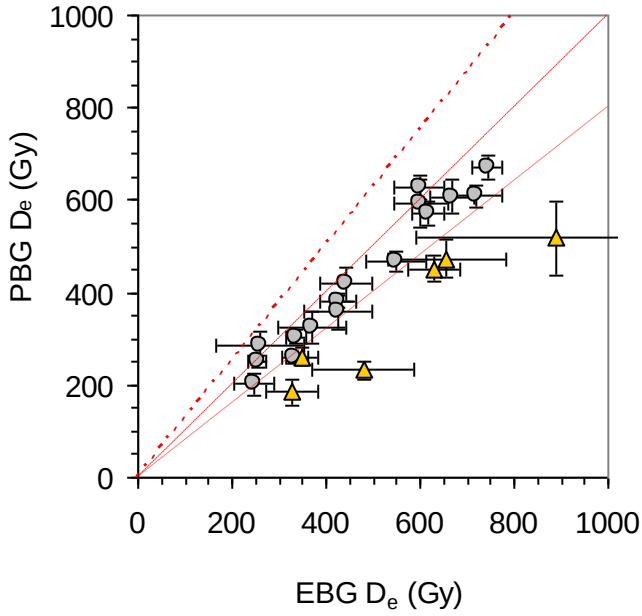
1000
800
600
400
200
0
PBG De (Gy)
0
200
400
600
800
1000
EBG De (Gy)

Fig. 11

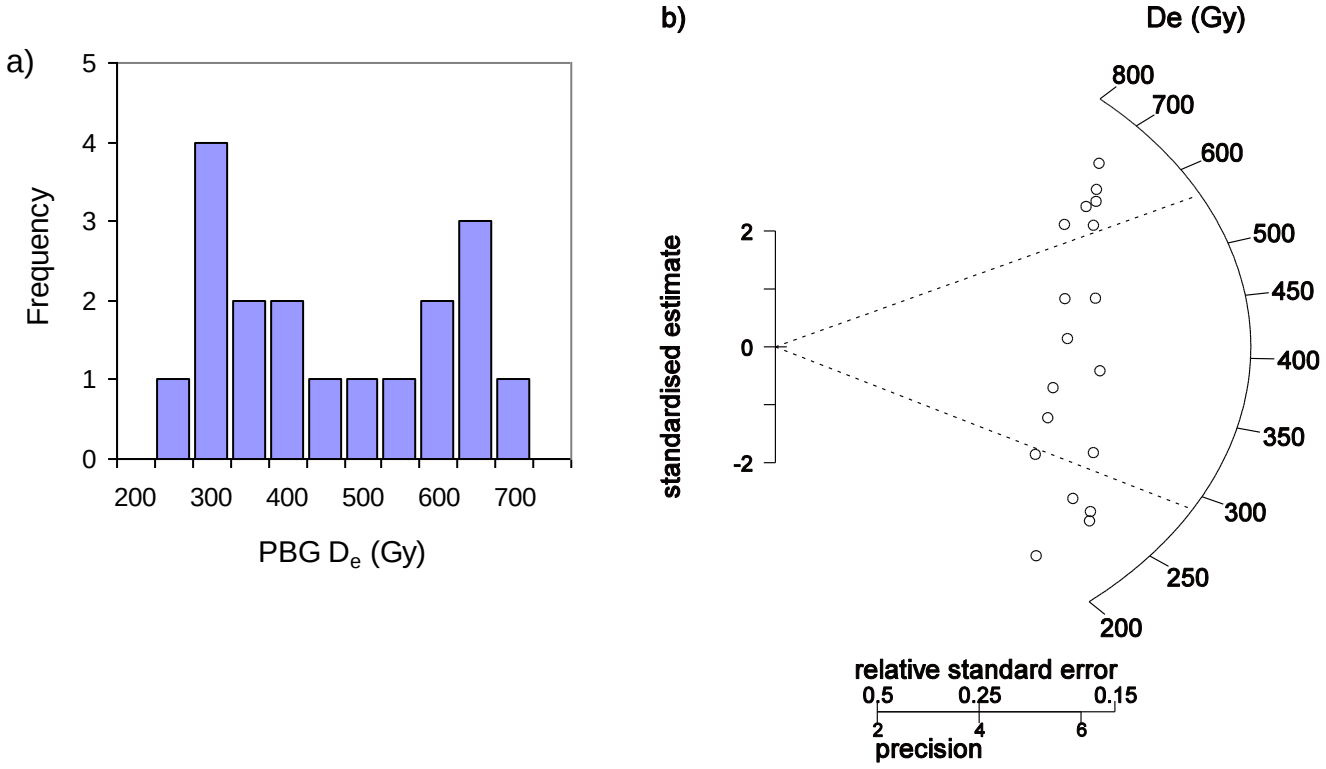
a)
5
4
3
2
1
0
Frequency
200
300
400
500
600
700
PBG De (Gy)
b)
De (Gy)
800
700
600
500
450
400
350
300
250
200
2
0
-2
standardised estimate
relative standard error
0.5
0.25
0.15
2
4
6
precision

Fig. 12

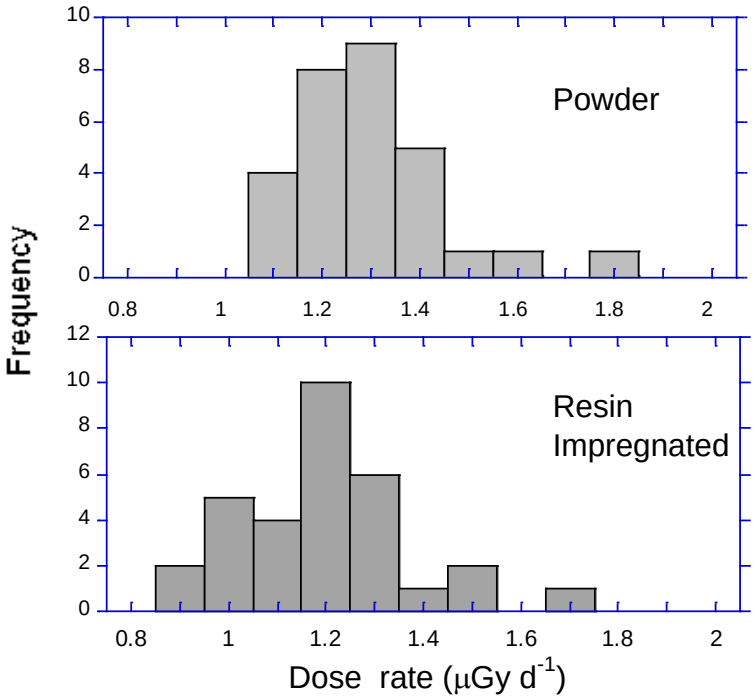
Frequency
Powder
Resin
Impregnated
Dose rate (μGy d-1)
0
2
4
6
8
10
12
0.8
1
1.2
1.4
1.6
1.8
2

Supplementary Material

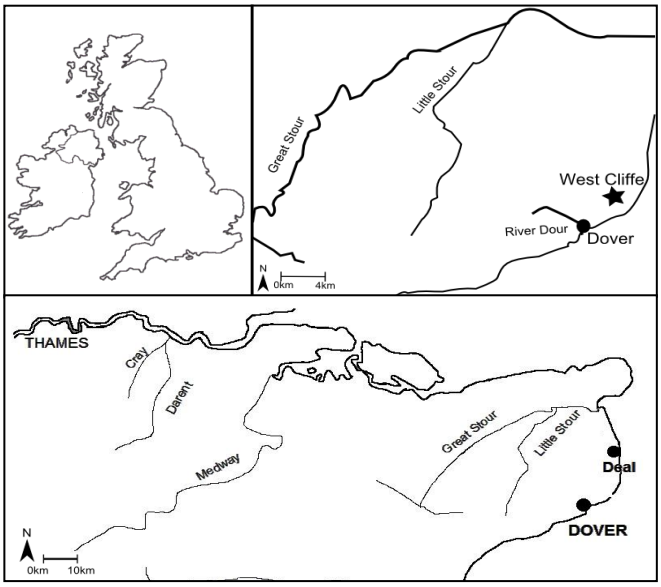

Figure SM1
Maps showing the location of the site at West Cliffe, St Margaret's, Kent.

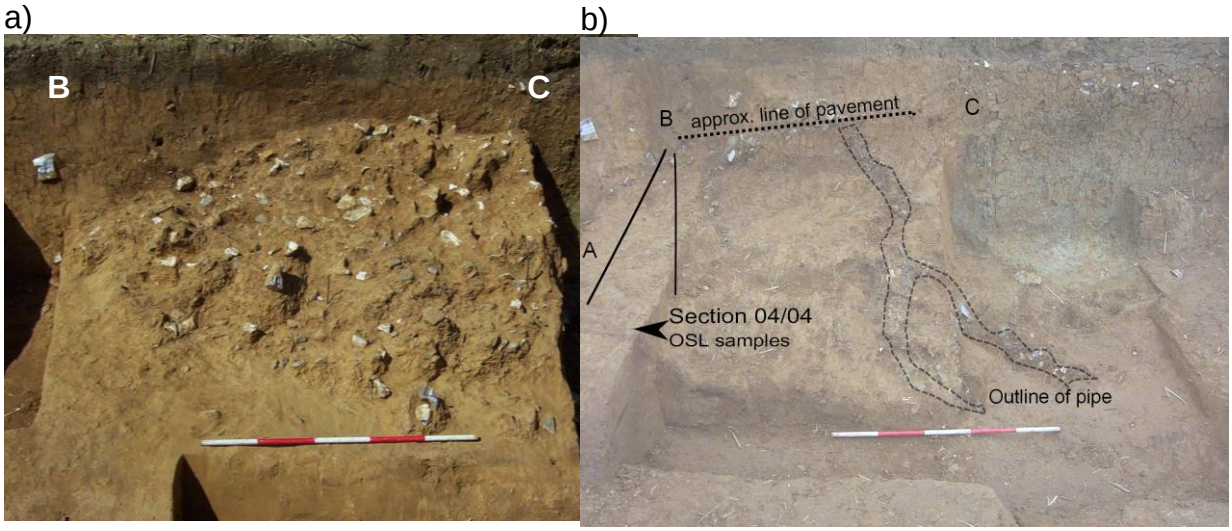

Figure SM2
View (a) of excavated cobble surface sloping into hollow in Area 1; view (b) of excavated surface that revealed a curving 'pipe' leading from the pavement and cobble layer in Area 1, and also indicating the orientation of Section 04/04 shown in Fig. 2a of the main text.

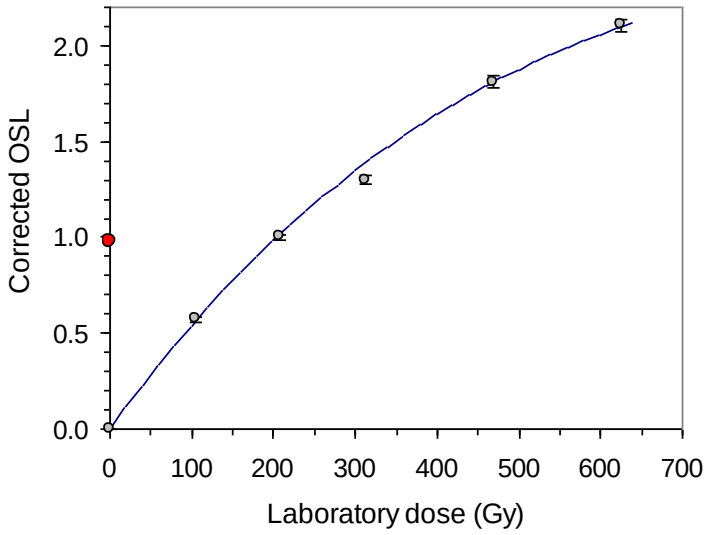

Figure SM3

Example of a dose response curve obtained using the SAR measurement procedure with an aliquot containing a dominant individual bright grain, as indicated subsequently by OSL scanning measurements. The value of the dose response parameter, D_0, is 544±34 Gy and the value of the equivalent dose, D_e, of 206±8 Gy was determined by the intersection of the value of the natural OSL (red filled circle) with the fitted dose response curve.

a)

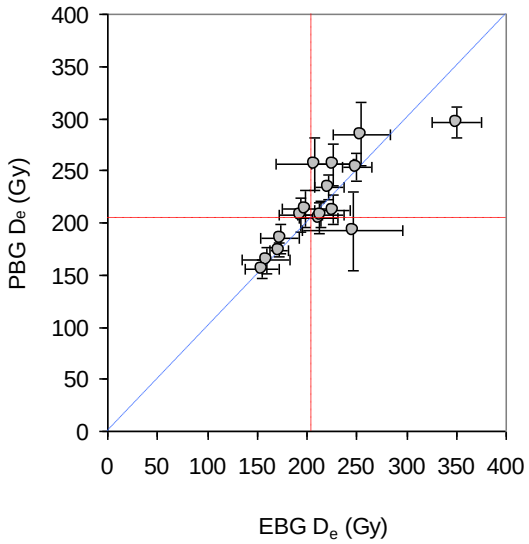

b)

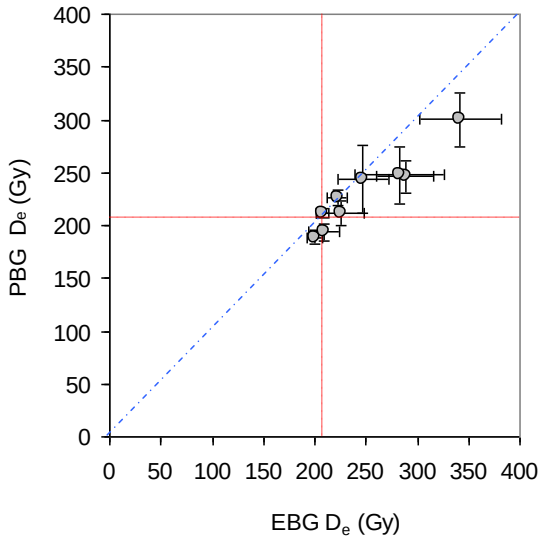

Figure SM4

Dose recovery experiment: comparison of D_e values obtained for very small aliquots, each containing a dominant individual bright grain, of samples a) 316-2 and b) 316-3 using the PBG and EBG subtraction procedures. The applied dose, D_a, is indicated by the dashed lines drawn parallel to each axis; with zero overdispersion the D_e values are expected to lie close to the point of intersection.

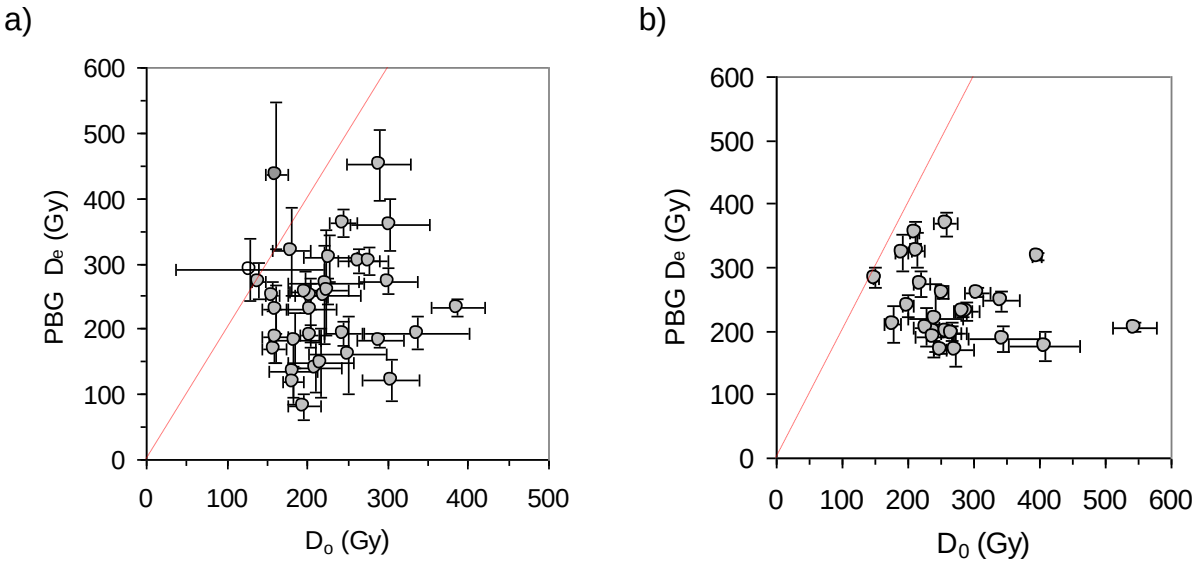

Figure SM5
Dose response characteristics measured with very small aliquots, each containing a dominant individual bright grain. The plots of D_e vs D_0 shown are for samples a) 316-2 and b) 316-3. The dashed lines correspond to the limit of the recommended working dose range, $D_e=2D_0$.

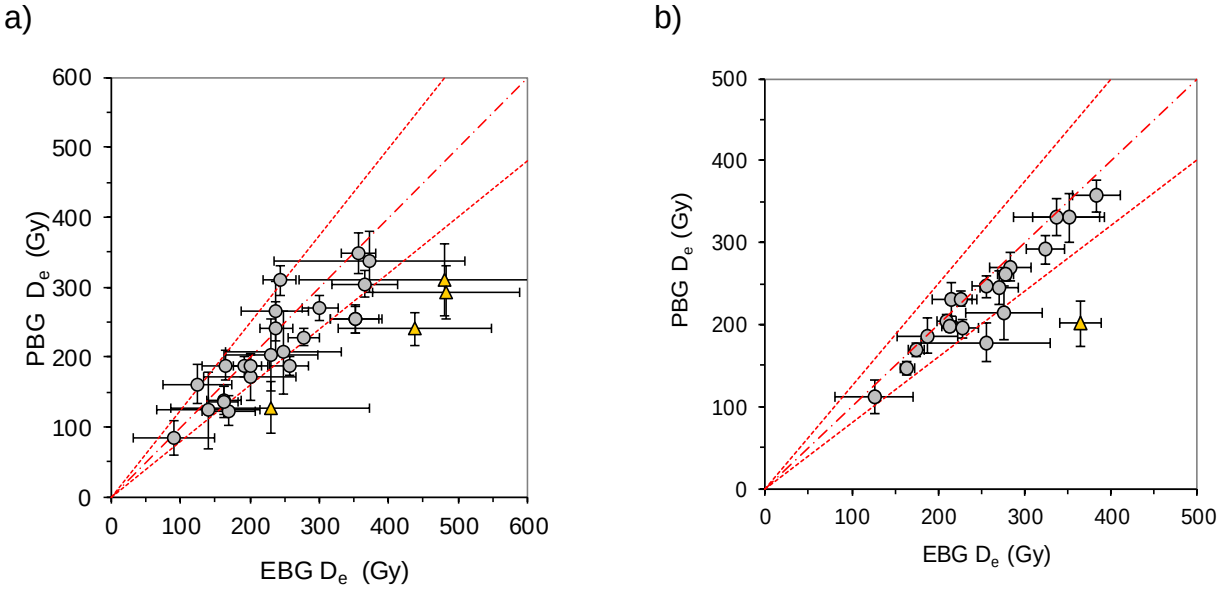

Figure SM6
Dose response characteristics measured with very small aliquots from samples a) 316-2, b) 316-3, each containing a dominant individual bright grain, where the plots show PBG D_e vs EBG D_e. The signal and background integration intervals were both 0-800 ms in the case of PBG subtraction and 0-800 ms and 800-1600 ms for EBG subtraction respectively. The filled triangle data symbols indicate exclusion from the calculation of the average D_e as discussed in the main text. The dashed lines correspond to ±20% of equivalence (dash-dot).

a(i)

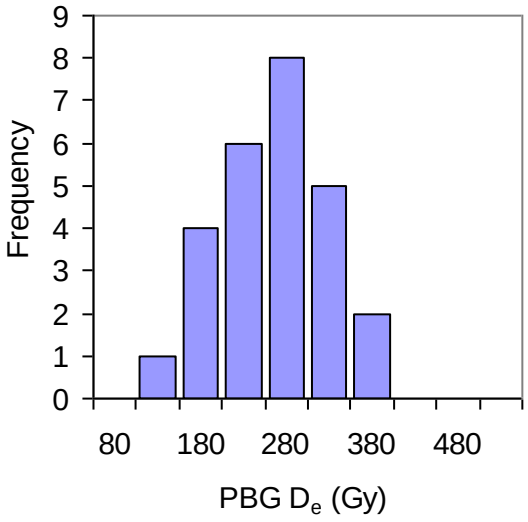
Frequency
0
1
2
3
4
5
6
7
8
9
80
180
280
380
480
PBG D_e (Gy)

a(ii)

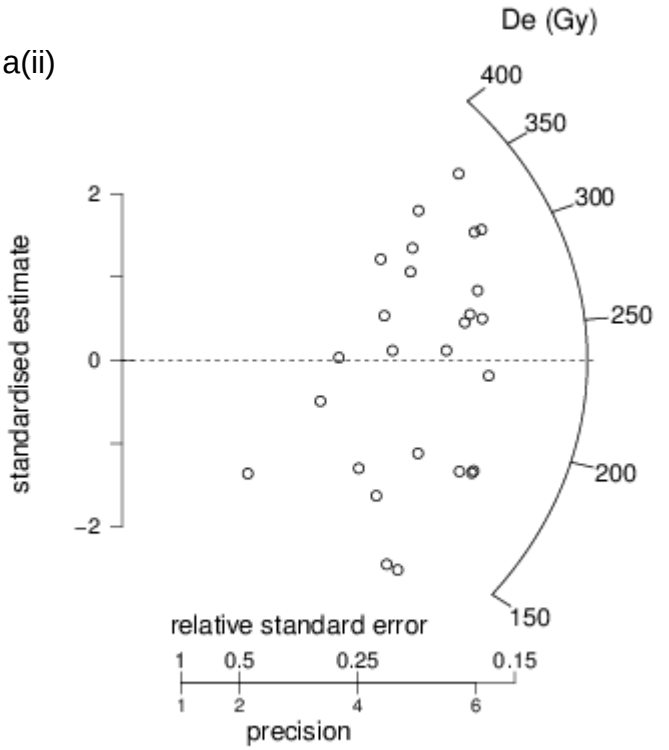
De (Gy)
400
350
300
250
200
150
standardised estimate
2
0
−2
relative standard error
1
0.5
0.25
0.15
1
2
4
6
precision

b(i)

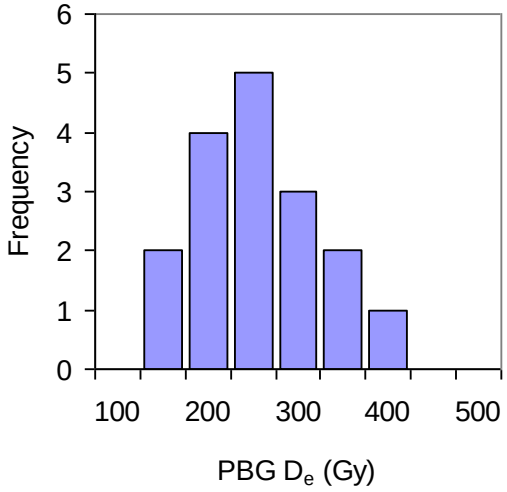
Frequency
0
1
2
3
4
5
6
100
200
300
400
500
PBG D_e (Gy)

b(ii)

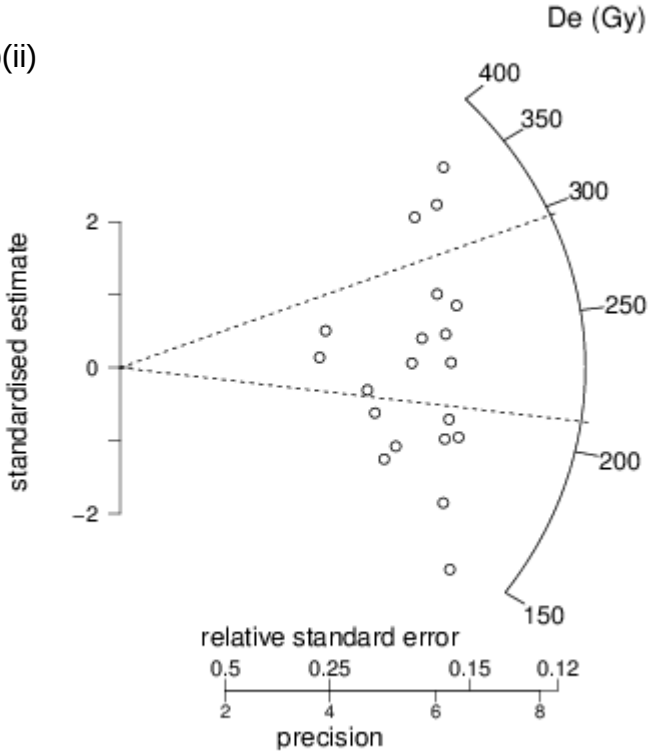
De (Gy)
400
350
300
250
200
150
standardised estimate
2
0
−2
relative standard error
0.5
0.25
0.15
0.12
2
4
6
8
precision

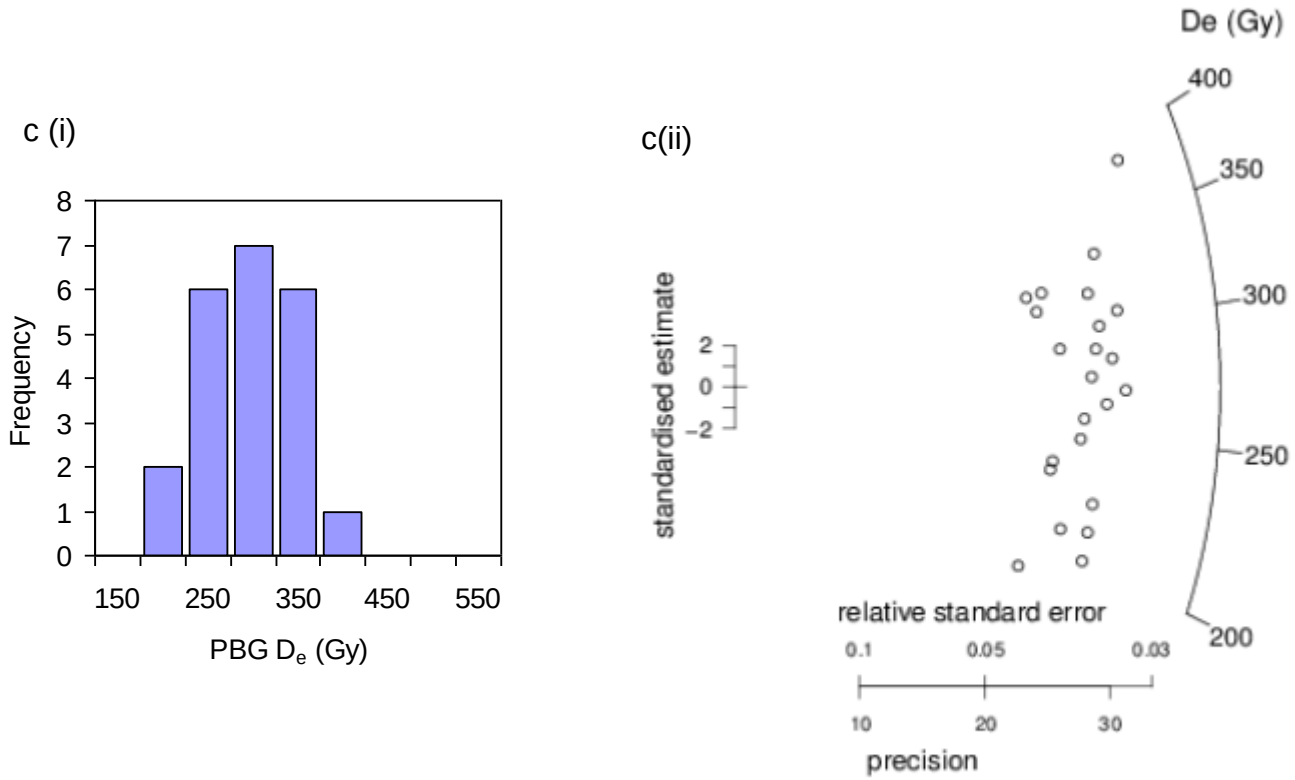

Figure SM7
Histograms (i) and radial plots (ii) of PBG D_e values shown in Fig. 10 of the main text that were used to calculate the weighted average for very small aliquots from samples a) 316-2 and b) 316-3, each containing an individual dominant bright grain, and c) small aliquots from sample 316-2. The broken lines indicate the value of the D_e components evaluated using the CDM (a) and FMM (b) models.